Geochronological and mineralizing fluid constraints associated with the Washita Valley Fault System

by

James Kenneth Phillips Rickert

B.S., Kansas State University, 2023

A THESIS

submitted in partial fulfillment of the requirements for the degree

MASTER OF SCIENCE

Department of Geology
College of Arts and Sciences

KANSAS STATE UNIVERSITY
Manhattan, Kansas

2025

Approved by:
Major Professor
Dr. Brice Lacroix

Copyright

Abstract

The Arbuckle Mountains, Oklahoma, correspond to an inverted aulacogen uplifted during the Pennsylvanian (320-290 Ma). The Arbuckle Mountains are affected by a large-scale strike-slip fault system: the Pennsylvanian Washita Valley Fault System. Based on stable (O, C) and radiogenic Strontium isotope approaches on carbonate rocks and veins, previous studies have attempted to resolve the syn-tectonic diagenetic and paleo fluid-flow history of the Arbuckle Mountains. Results from these studies suggest that the diagenetic alteration of carbonate exposed within the Arbuckle Mountains was dominated by meteoric fluid structurally channelized along fault systems.

Although the principal tectonic phase is linked to the Pennsylvanian Arbuckle Orogeny, two other deformation events have been documented on the field, suggesting a long lasting and complicated tectonic history, opening debate about the exact timing of the sinistral Washita Valley Fault System and its related paleo-fluid flow.

To resolve the exact timing of the Washita Valley Fault System activity, we performed detailed field-based structural analysis coupled with *in-situ* U-Pb analyses on fault related carbonate veins. In addition, we used conventional O and C stable, and Δ47 clumped isotope analyses on carbonate veins and their direct host rocks to document the associated fluid-related alteration. Our preliminary results suggest that the Washita Valley Fault was active during Early Cretaceous (140-109 Ma), contradicting previously proposed Pennsylvanian ages (320-290 Ma) estimated by either stratigraphic correlation or from seismic data interpretation. In addition, our new stable isotope data also suggest that the Washita Valley Fault System acted as an open hydrological fluid system involving marine and meteoric water at 44-68 ˚C during its activity.

Table of Contents

List of Figures

List of Tables

Acknowledgements

I would firstly like to acknowledge those who made this thesis possible and whom I worked with as a team. I would especially like to thank my advisor, Dr. Brice Lacroix, for his unwavering support and dedication to my studies and to my career. The experiences and opportunities I have had under Dr. Lacroix's advisement I have found invaluable and will continue to cherish as I go forward in my career. I would also like to acknowledge Pierre-Jean Hainque, who has joined me on trips to the field and whose insight and character was a great pleasure to be in the presence of. I also enjoyed being able to collaborate with master's student Bethsabee Tatischeff during trips to the Arbuckle Mountains, as well as on analytical tools at the University of Lausanne, and master's student Matt Arana during trips to the Arbuckle Mountains.

I would also like to acknowledge those who have made the master's degree journey even more enjoyable and insightful than it might've been otherwise. To Quinton Mindrup, Quinton Van Bever, Noellie Coeffier, Levi Pruitt, Wyatt Everhart, Logan Erichsen, and Quillen Thornton, every one of you has impacted me in a way that has brought light to my life during my undergraduate and graduate degree process. I appreciate you all greatly and wish you all success in your future endeavors.

I am extremely grateful to my family who have consistently supported me throughout my studies and beyond. To my mother and father, you both have been people I can come to with any concern, any issue, or any event in my life, with those things being returned with an atmosphere of objectiveness, support, and love. It is truly a privilege to be your son. I am also grateful to my grandparents, Terry Rickert and Beverly Rickert, Jim Phillips and Connie Phillips. They provided a model of ethics, respect, gratefulness, compassion, and motivation that survives in their children that I hope I can live up to. To the Long family, you have treated me as your own son since I was very little. You have fueled my interest in the natural world since that time. You have been a very critical part of my development, and I am very grateful to have you in my life.

I would also like to acknowledge the American Chemical Society for the funding it provided for this project, Sulphur, OK for hosting me several times during my research and which was unfortunately hit by a devastating tornado in April of 2024, and the Geology department of Kansas State University for its community.

Chapter 1 - Introduction

Faults compose major tectonic features well known to provide both preferential pathways for and barriers to fluid transport through basins, particularly hydrocarbons (e.g. Badertscher et al., 2002; Boles et al., 2004; Fitz-Diaz et al., 2011; Lacroix et al., 2014). Fault activity history can be simple, with frequency being as small as one single slippage event, or more complex involving several stages of reactivation in response to different tectonic stress regimes. One way to reach this goal is to study fault-related carbonate phases, which are regarded as indicative of paleo fluid-flow along fault zones (e.g. Badertscher et al., 2002; Boles et al., 2004; Fitz-Diaz et al., 2011; Lacroix et al., 2014; Trincal et al., 2017).

Conventional stable isotope (O, C and Sr) and fluid-inclusion microthermometric approaches analysis have been commonly applied to syn-tectonic carbonate veins to document paleo fluid-flow along fault zones and the associated diagenetic history in carbonate reservoirs (Goldstein and Reynolds, 1994; Lacroix et al., 2011, 2013, 2018; Mangenot et al., 2017). However, the application of these techniques may be limited by several factors. The determination of oxygen isotope composition of the precipitating fluid requires assumptions on the temperature conditions of the fluid and/or on the oxygen isotope composition of another cogenetic mineral phase (Chacko et al., 2001; Sharp, 2009). In a low-temperature environment (e.g., <100˚C), fluid inclusions, which can be used to retrieve paleo-temperatures, are not always present in carbonate phases. When they are, post-entrapment processes such as decrepitation can affect the reliability of this method (e.g. Mangenot et al., 2017).

Recently, syn-tectonic fluid-flow studies have been improved by the emergence of Δ47 clumped-isotope thermometry and U-Pb geochronology on carbonates (e.g. Lacroix et al., 2014; Mangenot et al., 2017; Hoareau et al., 2021; Beaudoin et al., 2022; Roberts et al., 2022; Betania

Palacios-García, 2023). Δ47 isotope thermometry allows estimation of both the absolute temperature of carbonate precipitation and the oxygen isotope composition of diagenetic fluid at the origin of carbonate precipitation without the temperature assumptions or the need of another cogenetic mineral phase. Recent development in *in situ* U-Pb dating of calcite cements provides the analytical and spatial resolution calcite cements associated with low-temperatures diagenetic processes and/or brittle faulting (Hansman et al., 2017; Nuriel et al., 2017; Ring and Gerdes, 2016; Roberts and Walker, 2016; Mangenot et al., 2018).

The WVFS corresponds to a series of NW-trending sinistral faults running through the Arbuckle Mountains, OK. The current structural interpretations of Oklahoma's Arbuckle Mountains region perceived the Washita Valley Fault as a Pennsylvanian-age sinistral strike-slip system (Ham, 1950; Carter, 1979; Allen, 2000; Turko & Mitra 2020; Turko & Tapp 2021). This age interpretation is restricted to relationships between graben formation from normal faults connected to the Washita Valley Fault and Virgilian-age infilling sediments (Ham, 1950; Carter, 1979; Allen, 2000; Turko & Mitra 2020; Turko & Tapp 2021). However, field observations have demonstrated that Pennsylvanian and post-Pennsylvanian sediments are crosscut by WNW oriented sinistral strike-slip faults, suggesting a more complicated history of the Washita Valley Fault System opening new debates (Ham, 1950; Carter, 1979; VanArsdale, 1989; Allen, 2000; Turko & Tapp 2021). In addition, the temperature conditions and the nature of fluid involved during fault activity has not been constrained yet, bringing some questions about the palaeohydrological behavior of the WVFS. To determine the absolute timing of deformation and the syn-tectonic fluid flow associated to the Washita Valley Fault system activity, we investigated fault-related veins and their associated paleofluid sources, petrography (cathodoluminescence and thin section microstructures), geochemistry (geochronological dating by U-Pb) and stable and clumped isotopes (O, C)), and performed structural and kinematic analysis on syn-tectonic structures (slickenfibers, veins, stylolites, striations, faults).

Chapter 2 - Geologic Setting

2.1 Regional Geologic Background:

The Arbuckle Mountains are an inverted aulacogen that consists of a N-NE vergent fold-and-thrust belt that resulted from the Pennsylvanian Wichita Uplift and Arbuckle Orogenic events (Ham 1964; Granath 1989, Thomas et al. 1991; Keller 2007; Turko & Tapp 2021). More particularly, the Arbuckle Mountains formed by a tectonic inversion of the South Oklahoma aulacogen; a Cambrian (535 Ma) aborted rifting phase of the supercontinent Rodina. The area consists of folded rocks from Precambrian and Cambrian granites through to Pennsylvanian sedimentary formations (Figure 1) (Ham, 1973; Fay, 1989; Granath 1989; Suneson 2014; Brueseke et al. 2016). The rift phase is contemporaneous with an important volcanic activity, marked by the formation of the Colbert Rhyolite and the formation of a flood basalt province, as well as a series of NW-trending extensional faults and grabens (Brewer 1985; Gilbert & McDonnel 1991: Keller 2014, Brueseke et al. 2016). This rift phase ultimately led to the closure of the Rheic and Paleo-Tethys oceans and the collision of the Gondwana and Laurentia supercontinents causing an inversion of the Southern Oklahoma Aulacogen structures and marks the beginning of the Pennsylvanian (320-290 Ma) Arbuckle, Ouachita-Marathon, and Appalachian Orogenies, and supplemented the deformation that resulted in the Ancestral Rocky Mountains (Kluth & Coney 1981; Kluth 1986; Budnik 1986; Thomas 1991; Poole, 2005; Keller 2007; Keller 2014; Leary 2017, Turko & Tapp 2021). The Pennsylvanian Orogeny is characterized by late Pennsylvanian syn-orogenic conglomerate deposition creating an angular unconformity with folded stratigraphic sequences.

Paleogeographic reconstruction suggests that the studied area was covered by the Western Interior Seaway (WIS), a shallow Cretaceous inland sea formed due to the subduction of the Farallon Plate beneath the North American plate (Kauffman 1985; Kauffman & Caldwell 1993; Roberts & Kirschbaum 1995; Slattery et al. 2013). This back-arc basin was then filled with marine water from both the Arctic Ocean and the Gulf of Mexico (Kauffman, 1985). The partial or total submersion of what is today the state of Oklahoma is illustrated via isopach and paleogeographic maps produced during periods of transgression in the Cretaceous (Figure 2). Whereas the exact timeframe of the existence of the Western Interior Seaway is still debated, marine sediment records indicate ages ranging between 145 and 59 Ma (Kauffman & Caldwell 1993; Slattery et al. 2013).

2.2 Tectonic Framework

Following the Cambrian rifting phase that resulted in the formation of the Southern Oklahoma Aulacogen, at least three different phases of deformation affecting the Arbuckle Mountains region have been recognized (Lacroix et al., 2022; Rickert et al., 2023). Shortening from the Pennsylvanian Orogeny (320-290 Ma) caused Northward thrusting and large-scale to parasitic style folding of the local stratigraphy (D_1) (Hessert, 2016). A Triassic post-orogenic extensional phase (270-240 Ma) that resulted in the formation of localized N-S normal faults offsetting the Arbuckle Anticline fold axis (D_2) has recently been documented. Finally, the third phase corresponds to the sinistral Washita Valley Fault activity described in more detail within section 2.3 (D_3). Based on seismic data interpretation, previous studies suggest that the Washita Valley Fault System formed during the late Pennsylvanian orogenic event in response to a slight change in the main horizontal stress (Turko & Tapp 2021). Note that the D_2 and D_3 deformation events are based on a collection of currently unpublished structural and geochronological data.

2.3 Washita Valley Fault System

The Washita Valley Fault System is a primarily left lateral strike-slip system oriented NW-SE (Figure 1). The estimated lateral offset, which varies from 1-3 miles (Ham, 1950; Dunham 1955) to 20-40 miles, (Tanner, 1967; Carter, 1979; Webster, 1980; Booth 1982; Brown and Grayson, 1985) has been determined based on stratigraphic offsets within both the Simpson and Hunton Groups. The relative age of the Washita Valley Fault has been proposed as Pennsylvanian based on cross-cutting relationships within the late Pennsylvanian Collins Ranch Conglomerate as well as Permian sedimentary units (Figure 1) (Ham, 1950; Dunham, 1955; Turko & Mitra 2020; Turko & Tapp 2021). The Washita Valley Fault System is assumed to be produced by the reactivation of early Southern Oklahoma Aulacogen faults during the late Pennsylvanian as the stress-field rotated to the east-northeast from a northeast–southeast position (Thomas 1991; Turko & Tapp 2021). Note that such direction is consistent with the horizontal stress field associated with the early Pennsylvanian Arbuckle and Wichita Mountains orogenies (Granath 1989; Turko 2019; Turko & Mitra 2020; Turko & Tapp 2021). Although no field evidence exists, the combination of strike-slip and dip-slip movement is thought to have resulted in the formation of grabens in proximity to the Washita Valley Fault filled with Virgilian age (303-299Ma) sediments indicating the timing of displacement (Ham, 1950; Carter, 1979; Allen, 2000; Turko & Mitra 2020; Turko & Tapp 2021). However, fault offsets have also been observed within Virgilian and Cretaceous age sediments opening the debate of multi-stage activity of the Washita Valley Fault System (Ham, 1950; Carter, 1979; VanArsdale, 1989; Allen, 2000; Turko & Mitra 2020; Turko & Tapp 2021).

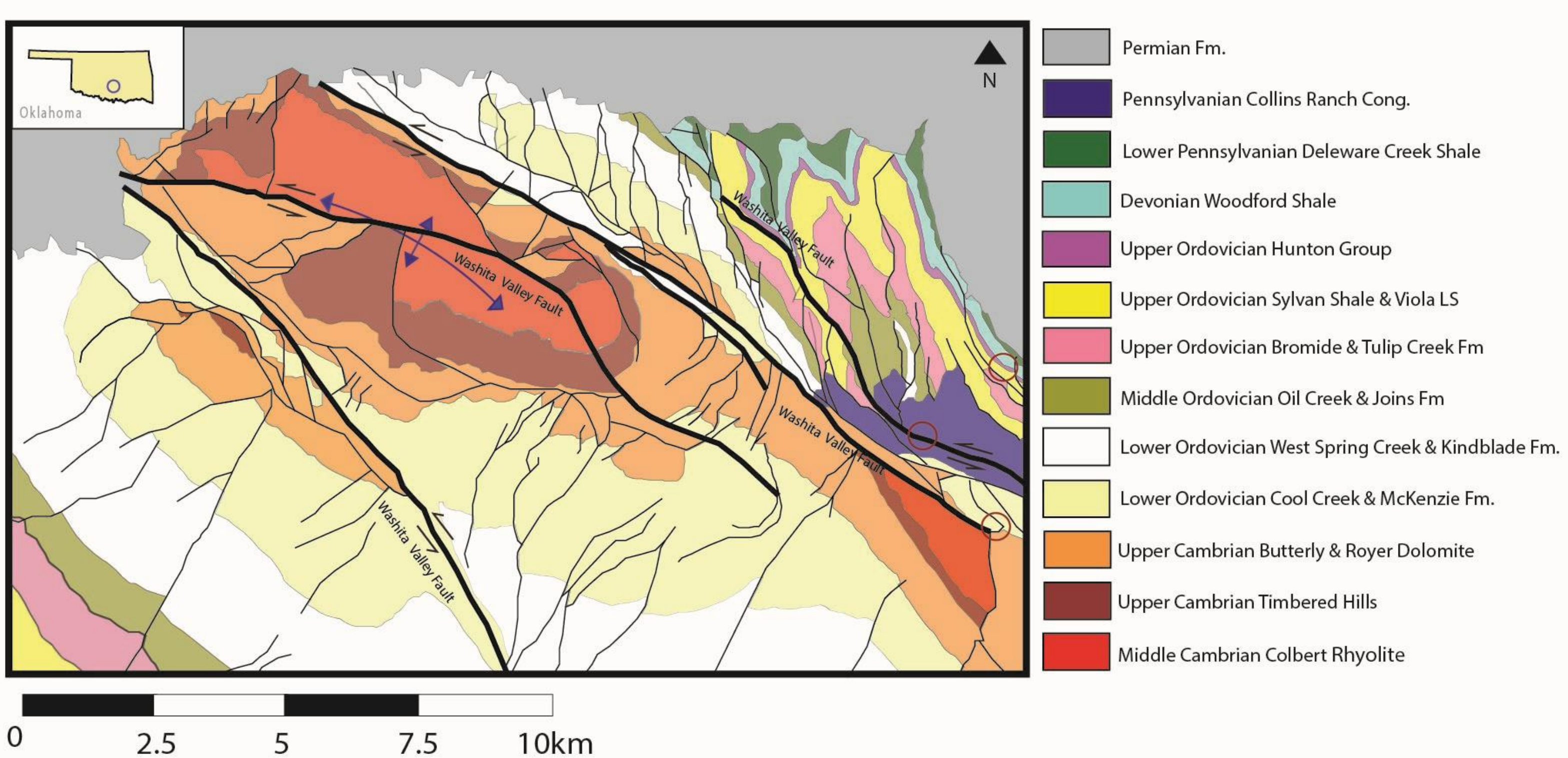

Figure 1: Geological Map of the Arbuckle Mountain modified from Ham, (1954), & Fay, (1989). Red circles indicate sample locations.

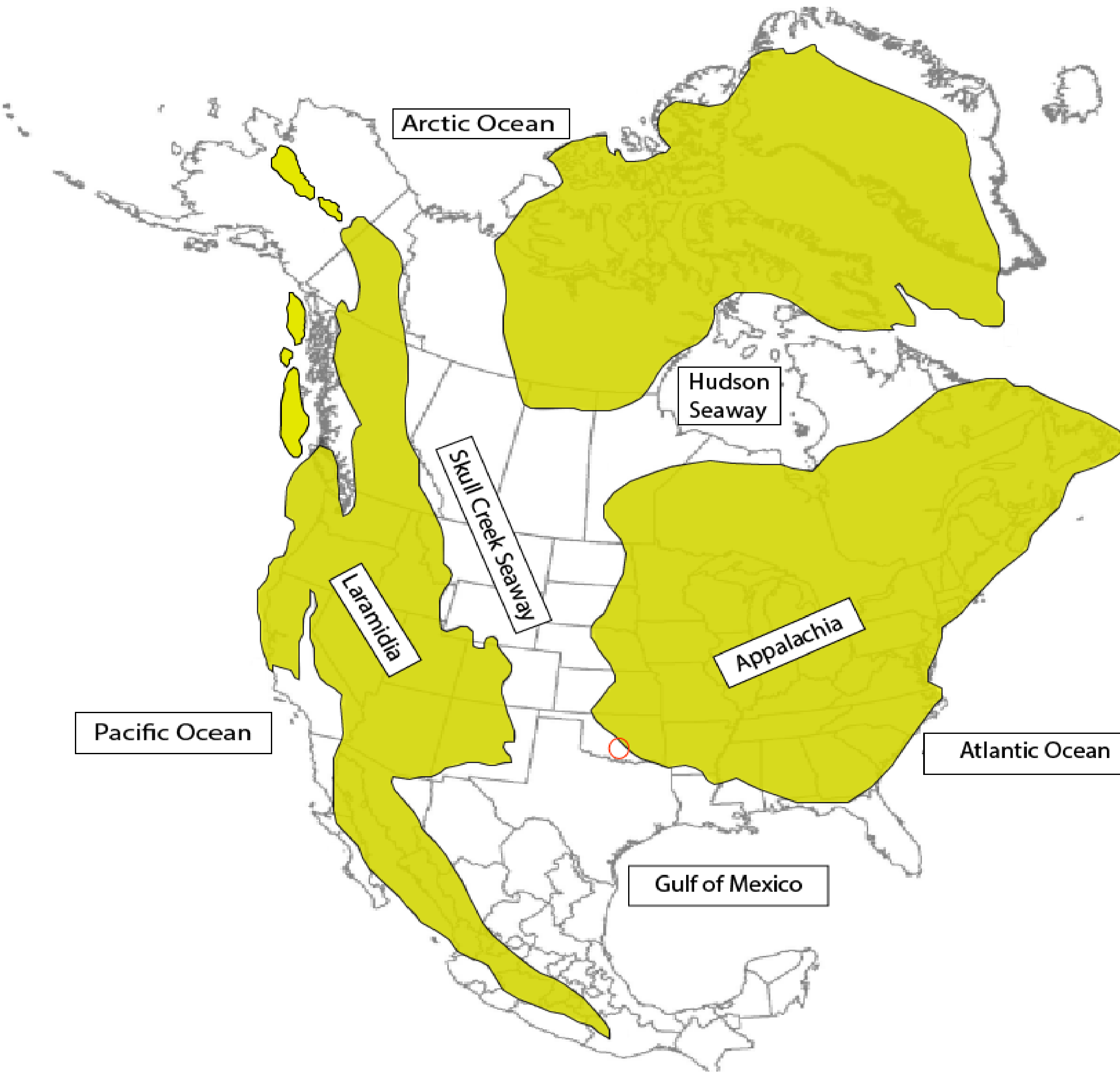

Figure 2: Cretaceous (113 Ma) paleogeographic map of North America modified from (Slattery et al. 2013). Yellow indicates continental crust. The red circle indicates the Arbuckle Mountain Region.

3.1 Sample Collection and Processing

Detailed outcrop scale structural analysis was performed on fault-related calcite veins, fault planes, and fault striations to ensure that selected strike-slip fault planes and associated calcite veins formed under the same stress-field as the Washita Valley Fault System tectonic event, D_3. Although many D_3-related fault planes did not feature slickensides; striations were visible for structural interpretation. Extension veins with the appropriate E-W orientation associated with the Washita Valley Fault System were systematically collected. For comparison, we did also collect calcite veins related to the Pennsylvanian Orogeny (D_1). Collected D_1-related samples include both bedding parallel slickenfibers and extension veins. 30 and 70µm polished thin and thick sections were prepared by National Petrographic Service, INC for Laser Ablation Inductively Coupled Plasma Mass Spectrometry (LA-ICP-MS).

3.2 Optical and Cathodoluminescence Microscopy

To distinguish the tectonic event and isolate Washita Valley Fault syn-tectonic features, relative geochronology of the collected samples was determined at the outcrop and micro scale through petrographic and cathodoluminescence (CL) microscopy. Micro and macro structures were identified within thin sections using optical petrographic and cathodoluminescence microscopes at Kansas State University to document the different generations of calcite mineralization and zoning. CL observations were made using a Nuclide Luminoscope operated at 8-16 kV and 4-.8 mA with an unfocused cold cathode electron beam in a vacuum chamber at 0.08-0.1 torr coupled to a Nikon Eclipse petrographic microscope equipped with a camera.

3.3 LA-ICP-MS U-Pb Dating

In-situ LA-ICP-MS analyses were performed on 7 vein samples from the Washita Valley Fault System, as well as the Pennsylvanian Orogeny for comparison, to produce absolute age timeframe. Analyses were performed at the University of Kansas and University of Pau, France. At the University of Kansas, a Thermo-Scientific Element 2 high resolution sector-field ICP-MS combined with an ANALYTE.G2 excimer laser at a 193nm wavelength was used to determine the absolute U-Pb geochronology of the analyzed generations of calcite mineralization observed in thin section. At University of Pau, age data for one sample was collected using the virtual spot approach technique described in Hoareau et al. (2024), which uses a high repetition rate femtosecond laser ablation system. 85 µm diameter laser spot locations were selected via CL crystal to document growth zonation when visible in thin section and avoid zonation overlap of a spot, as well as to avoid fractures, fluid inclusions, and sulfide minerals within the carbonate when possible. Anywhere from 15-80 laser spots were selected per thin section based on vein generations present and vein thickness, as well as the general quality of calcite. In addition, laser spots were selected within the mineralization host rock for comparison in the event of host rock inclusion within a vein.

U-Pb ages were determined from standard Terra-Wasserburg Concordia plot lower intercepts at a 2σ standard deviation. Data was excluded from age calculation at uncertainties ≥ 20%, based on post-analysis petrographic observation in case of fracture, fluid inclusion, or sulfide mineral overlap with a laser spot. In the case of these occurrences, the data did not lie on the isochron and caused a higher degree of uncertainty for the age calculation (e.g. Roberts et al. 2020). U-Pb ratios were determined using methods published on in-situ carbonates (Roberts et al. 2017, Roberts et al. 2020, Hoareau et al. 2021, Betania Palacios-García et al. 2023). "Unknown" calcite samples were bracketed by 3-5 carbonate reference materials, DBTL limestone (Hill et al., 2016) and WC-1 (Roberts et al. 2017), used to calibrate the U-Pb fractionation correction with an inhouse Excel spreadsheet. Baseline subtraction, Pb isotope fractionation, downhole fraction and drift corrections were done via the Iolite program (Paton et al., 2010; Paton et al., 2011) using NIST612 (glass) reference material (Jochum et al., 2011).

Analyses of calcite requires the consideration of the presence of initial/common Pb in the system during vein mineralization. Initial/common Pb typically exists in variably high quantities within carbonate (Roberts et al. 2017), which requires the use of a Tera-Wasserburg diagram to account for the offset from the lower Concordia intercept created by the initial/common Pb. An absolute age is determined by the lower intercept between the isochron and the Concordia, which is representative of radiogenic Pb, as opposed to the upper intercept that is indicative of initial/common Pb.

3.4 Stable Isotope Analyses

3.4.1 C and O Isotope Analyses of Carbonates

Calcite veins from the Washita valley Fault and their host carbonates were analyzed to determine the carbon and oxygen stable isotopic composition. For this, calcite veins and host rocks were systematically powdered with a handheld Dremel micro drill. The C and O isotopic composition of the sampled carbonates were measured via a GasBench II connected to a Finnigan MAT Delta V mass spectrometer, using a He gas carrier system adapted from methods from Spoetl and Vennemann (2003). Carbonates are reacted with orthophosphoric acid for a total of 1 hour at a temperature of 70 ºC. All samples are normalized using an in-house standard (Carrara Marble) calibrated against $\delta^{13}C$ and $\delta^{18}O$ values of NBS-19 (+1.95 and –2.20 ‰, relative to Vienna Pee Dee Belemnite - VPDB). External reproducibility for the analyses is estimated from replicates of the in-house standards (n=10) was calculated to be ±0.05 ‰ for $\delta^{13}C$ and ±0.04 ‰ for $\delta^{18}O$. Fractionation for oxygen isotopes was corrected for using methods derived from O’Neil et al. (1969) and Zheng et al. (1998).

3.4.2 Δ_{47} Clumped stable isotope analyses of carbonates

Six carbonate vein samples from the Washita Valley Fault System were powdered for a weight of 3500 – 4500 µg and then packed into 2 ml vials for further analysis. Clumped isotope measurements were conducted at the University of Lausanne using a NuCarb sample preparation device coupled to a Nu-Perspective gas source mass spectrometer. Between 400 and 600 µg of carbonate was reacted with 110 µl of injected H_3PO_4 (SG of 1.95) at 70°C for 45 minutes. The extracted gas was first transported across a water trap held at –80 ºC and through a PoraPakTM Q adsorption trap held at –30 ºC during extraction and then degassed at 150 ºC between sample extractions. then purified a second time into another liquid nitrogen cooled cold finger on the dual inlet of the mass spectrometer. These analyses commonly have precision better than 0.02 and 0.04 ‰ for $\delta^{13}C$ and $\delta^{18}O$ values (1 STDEV), respectively, for the in-house Carrara Marble RM (CM2), and NBS-19 and -18 used for normalization. Δ_{47} clumped isotope measurements of 300 to 800 µg-sized samples have a typical standard deviation (1 SD) of 0.007 to 0.012 ‰ and between-run external standard deviations for CM2, ETH-1, and ETH-3 of 0.015 ‰ (n = 9), or 0.020 ‰ for ETH-2 and -4 (n = 3), while for large samples of about 4 mg, the standard deviations are generally better than 0.008 ‰. A δ^{47}–Δ_{47} linearity correction as well as background or pressure baseline correction are not required and the final values are normalised relative to the carbonate RM's: ETH-1, -2, and -3, analysed at the start and end of each analysis sequence (Bernasconi et al., 2021). Final Δ_{47} values are normalised to the InterCarb 'carbon dioxide equilibration scale' (Δ_{47} I-CDES) (Bernasconi et al., 2021) using the slope and intercept of the Δ_{47} values of ETH-1, ETH-2 and ETH-3 (Bernasconi et al., 2018) projected to a 90 ºC acid temperature, applying an acid fractionation correction of 0.088 ‰ (Petersen et al., 2019; Bernasconi et al., 2021). Measured Δ47 values were transferred into the CDES Δ47CDES90 reference frame (Ghosh et al., 2006). Temperatures (T) are computed using the unified Δ_{47}-T calibration of Anderson et al. (2021), which is valid for a range of temperatures (0.5 ºC to 1100 ºC) and chemical compositions of carbonates (Anderson et al., 2021). Oxygen isotope compositions of water (δ^{18}Ow) are calculated by inserting the Δ_{47}-based temperatures and measured carbonate $^{18}O/^{16}O$ compositions into the widely accepted oxygen isotope thermometry equation of Kim and O'Neil (1997), applying a correction for CO_2-calcite acid fractionation factor of 10.25 (Kim and O'Neil, 1997). The universal calibration for all (Ca, Mg, Fe) CO3 carbonates proposed by (Bonifacie et al., 2017) was then used. Δ_{47}CDES90 data were converted to temperature (˚C) using the Bonifacie et al. (2017) calibration (Equation 1) and Anderson et al. 2021 (Equation 2) for carbonates:

$$\Delta_{47}CDES_{90} = 0.0422 * 10^6/T^2 + 0.1262$$

Equation 1: Calibration for carbonates according to (Bonifacie et al., 2017)

$$\Delta_{47}CDES_{90} = 0.0391 * 10^6/T^2 + 0.154$$

Equation 2: Calibration for carbonates according to (Anderson et al., 2021)

Oxygen isotope composition of paleo-fluid was determined using both O'Neil et al. (1969) and Zheng et al. (1998) oxygen fractionation equations and Δ47 temperature. Fluid compositions are reported in δ^{18}O Vienna Standard Mean Ocean Water (VSMOW).

Chapter 4 - Results

4.1 Structural Analysis

Based on structural observations made on outcrops and on samples, three main tectonic phases (D_1, D_2 and D_3) of variable intensity are distinguished. For ease of reference, we describe the structures related to each deformation event below. However, the primary focus is the Washita Valley Fault System.

4.1.1. D_1 Structures

Several structures related to D_1 events have been observed at regional scale. The bedding (S_0) is affected by a regional fold oriented NW-SE (N316). The fold stereographic analysis performed on bedding suggests that the bedding is affected by the aforementioned regional fold plunging 13˚ to N 316. Folds are generally asymmetric, North-verging, with long limb shallowly dipping to the South, and steep short limbs either steeply dipping to the North or overturned. Fold-hinge type extension veins striking NW-SE hinge type extension veins striking NW-SE subparallel to measured fold axes have been observed (Figure 3). Whereas sediments are affected by early stylolites ($styl_0$) parallel to bedding, they also feature another population of stylolites oriented N310/71 ($styl_1$) in agreement with a NE-SW tectonic stress direction (Figure 3). Bedding-parallel veins (SV1) are commonly observed along fold limbs (e.g., Figure 3). Such structures are formed by flexural slippage during folding events. Mode I extension veins, EV1, are also common and are oriented N028/67. Along shallowly dipping bedding (long-fold limbs), they define two “en-echelon” arrays oriented N065 and N072 (Figure 3). All these structures formed under the same stress-field in response to shortening oriented NE-SW (Figure 3).

The Collins Ranch Conglomerate (Figure 1) forms an angular unconformity with folded pre-Pennsylvania stratigraphy, and also displays evidence of open folding, which presumes late orogenic deposition during the Pennsylvanian.

4.1.2 D_2 structures

D_2 structures have been observed on a local scale and is defined by a series of Triassic normal faults oriented N 187/88 and evidenced by mm to cm thick slickensides (indicating normal movement) (Lacroix et al., 2022; Rickert et al., 2023). It is currently uncertain of the cause of the stress associated with this deformation event, however post-orogenic collapse can be excluded due to the discrepancy in U-Pb ages between Pennsylvanian shortening and Triassic extension from unpublished data (Lacroix et al., 2022; Rickert et al., 2023).

4.1.3 D_3 structures

The third phase consists of sinistral strike-slip faults striking E-W and WNW-ESE, consistent with previously mapped regional scale Washita Valley Faults (Figure 1). It is important to note that some observed strike-slip faults cross-cut Pennsylvanian age stratigraphy (Figure 1 and 4) and higher densities of Washita Valley Faults are present along the North limb of the Arbuckle anticline where the local stratigraphy is sub-vertical. Fault planes frequently display sub-horizontal striations and/or slickenlines (Figure 4). Although, Washita Valley fault planes do not systematically display slickensides, when present, they indicate sinistral movement (Figure 4). Isolated or “en-echelon” extension veins (EV3) oriented N110/82 have been observed at proximity of Washita Valley Fault System and are commonly associated with a set of N-S oriented stylolites (styl3) (Figure 4). Strike-slip faults, striations, slickensides, extension veins (EV3) and tectonic stylolites (styl3) are all consistent with a maximum horizontal stress oriented E-W (Figure 4). During sampling, EV3 veins were much more brittle than those associated with

NE-SW D_1 shortening. The latter appear more solid-milky white as opposed to Washita Valley Fault related veins which appear clearer to colorless.

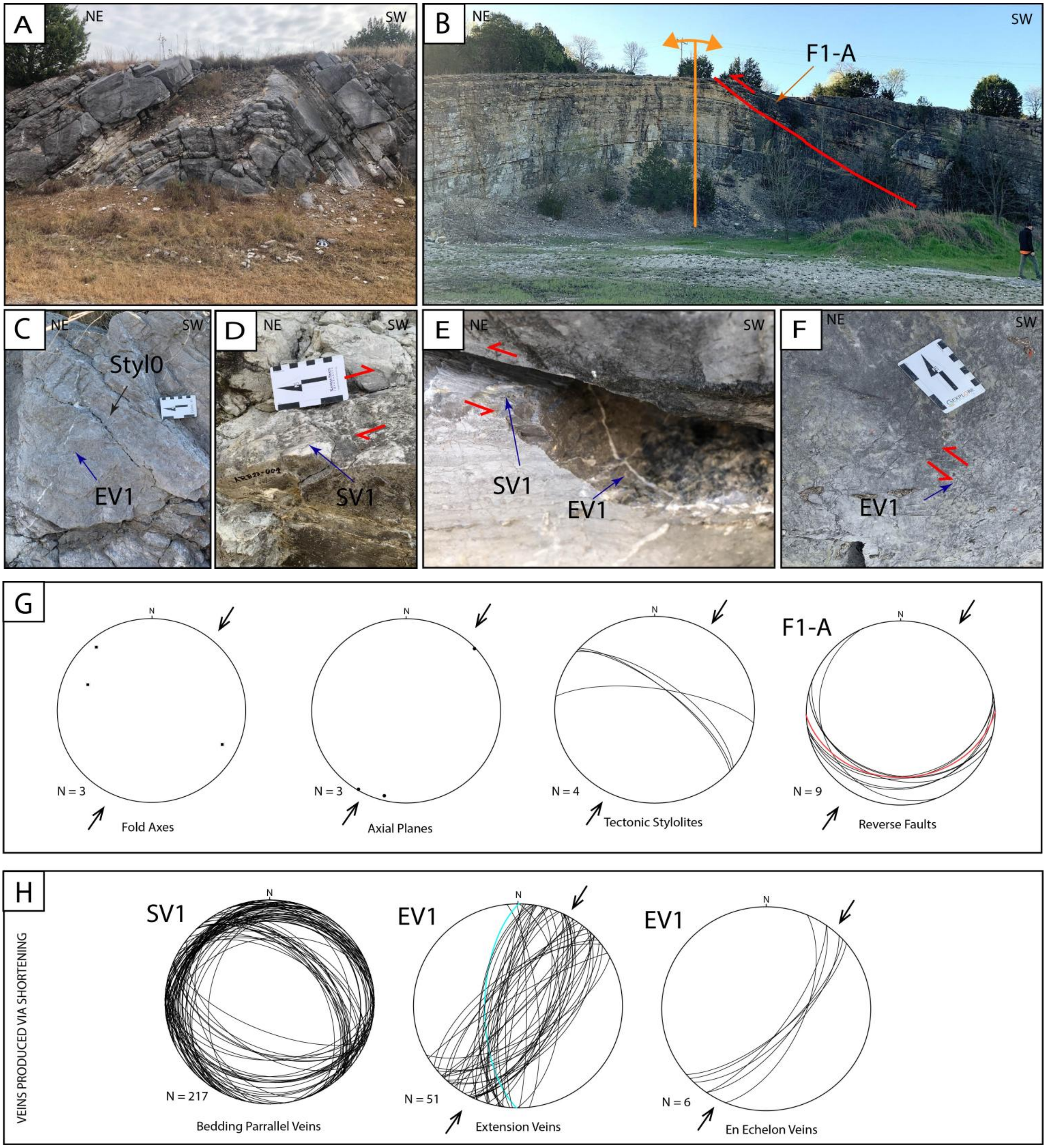

Figure 3: Field outcrops depicting Pennsylvanian Arbuckle Orogeny features. Pictures (A) & (B) depict anticlines and thrust faults (G) typical from fold-and-thrust type regimes (F1-A). Pictures (D) & (E) display bedding parallel slickensides representative of flexaral slippage during a shortening event (SV1). Pictures (C) & (E) display fold-hinge type extension veins with NW-SE orientation, while picture (F) displays en echelon veins (EV1-3) refelective of the primary stress visualized by the black arrows in pictures (G) and (H).

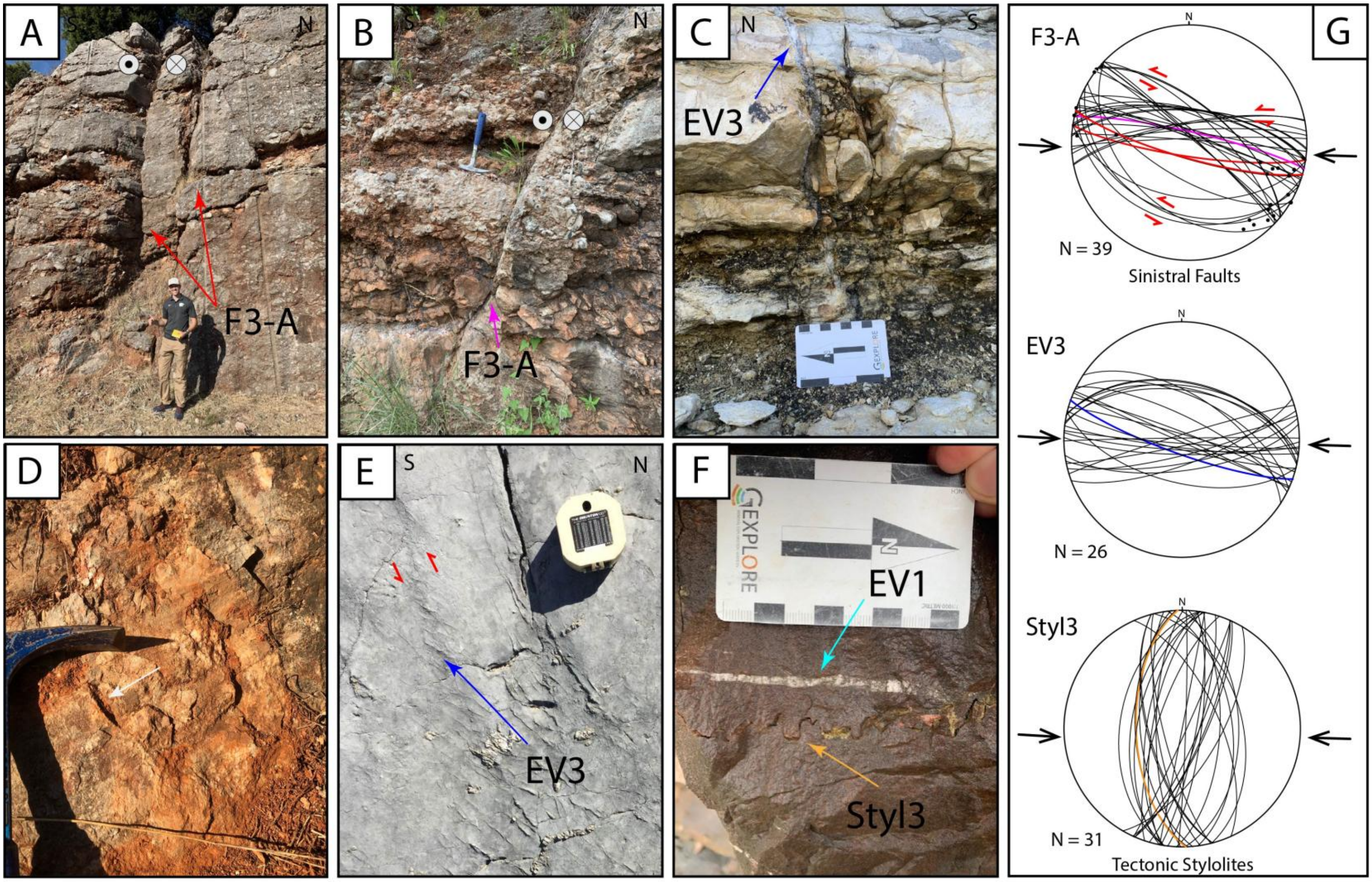

Figure 4: Field outcrops depicting features related to Washita Valley Fault System deformation. Pictures (A) & (B) depict sinistral faults (F3-A) containing slickensides from picture (D) oriented WNW-ESE within the Collins Ranch Conglomerate unit (Figure 1). Pictures (C) & (E) depict extension vein (C) and en echelon vein (E) (EV3-B) features indicative of the primary stress of the Washita Valley Fault System visualized by the black arrows in image (G). Image (F) depicts a subparallel relationship between D1 shortening veins and D3 Washita Valley Fault tectonic stylolites.

4.2 Petrographic Study

4.2.1 Microstructures

Petrographic and cathodoluminescence (CL) observations allowed for the identification of microstructures, twinning relationships, and zoning features within collected veins.

D1-related veins (SV1 and EV1)

The bedding parallel slickensides (SV1) corresponds to cm-thick tabular calcite veins with metric lateral extensions. They feature surface striations (slickenlines) and slickensteps both characteristics of slickensides (Figure 4D). Microscopically, they consist of stacked mm-thick layers of calcite separated by dark inclusion trails (Figure 5). Each layer is formed by a lateral succession of rhomb-shaped veinlets and, occasionally, host rock fragments that have fractured away from the host rock-vein boundary. Inclusions trails correspond to Mode 2 shear surfaces, whereas rhomb-shaped veinlets correspond to mode I extensional fracture sub-perpendicular to the surrounding stylolites (styl1). Sense of shear was determined via rhombus shaped “steps” of calcite which correspond to crack-seal void filling at pull-apart openings along bedding planes.

EV1 associated with the Arbuckle Orogeny consist of mm-thick veinlets mainly filled with white calcite, although the presence of celestine has been also observed. EV1 exhibit crack-seal type textures described in Bons et al. (2012) which indicate the precipitation of calcite coeval to the vein opening. Calcite cement is affected by a large density of thin calcite twins (Figure 5) which are interpreted as Type 1 twins based on Ferril’s classification scheme (Ferril 1991). Such twins are usually formed in low-temperature environment (<200˚C) (Ferrill et al., 2004). Veins associated with D_1 exhibit a higher density of twinning relative to veins associated with the Washita Valley Fault System (Figure 5).

Cathodoluminescence observations made on both EV1 and SV1 veins do not highlight clear evidence of zonings, but rather the presence of bright yellow CL along calcite twinning and grain boundaries. Such pattern is commonly associated to post-precipitation alteration of calcite along grain boundaries (Figure 6 A).

D3-related veins (SV3 and EV3)

Slickensides associated with the Washita Valley Fault System (SV3) correspond to mm to cm thick veins. They show similar features as for SV1 and consist of stacked mm-thick layers of calcite separated by inclusion trails opened by a combination of incremental Mode II shear surfaces slippage and Mode I openings (Figure 4 D).

Mode 1 veins associated with the Washita Valley Fault System (EV3) correspond to 0.8 mm to 1 cm thick syntaxial veins filled with granular-blocky and elongate-blocky calcite (Figure 5B). The presence of crack-seal type textures is also observed within EV3 indicating the precipitation of calcite coeval to the vein opening. Interestingly, no calcite twins have been observed within calcite cements, suggesting an even lower temperature of calcite precipitation than for D_1 veins (Ferrill 1991). Cathodoluminescence observations made in EV3 veins reveal the presence of complex zonings alternating bright and dull CLs, suggesting a fluid composition cyclicity during calcite precipitation (Figure 6B).

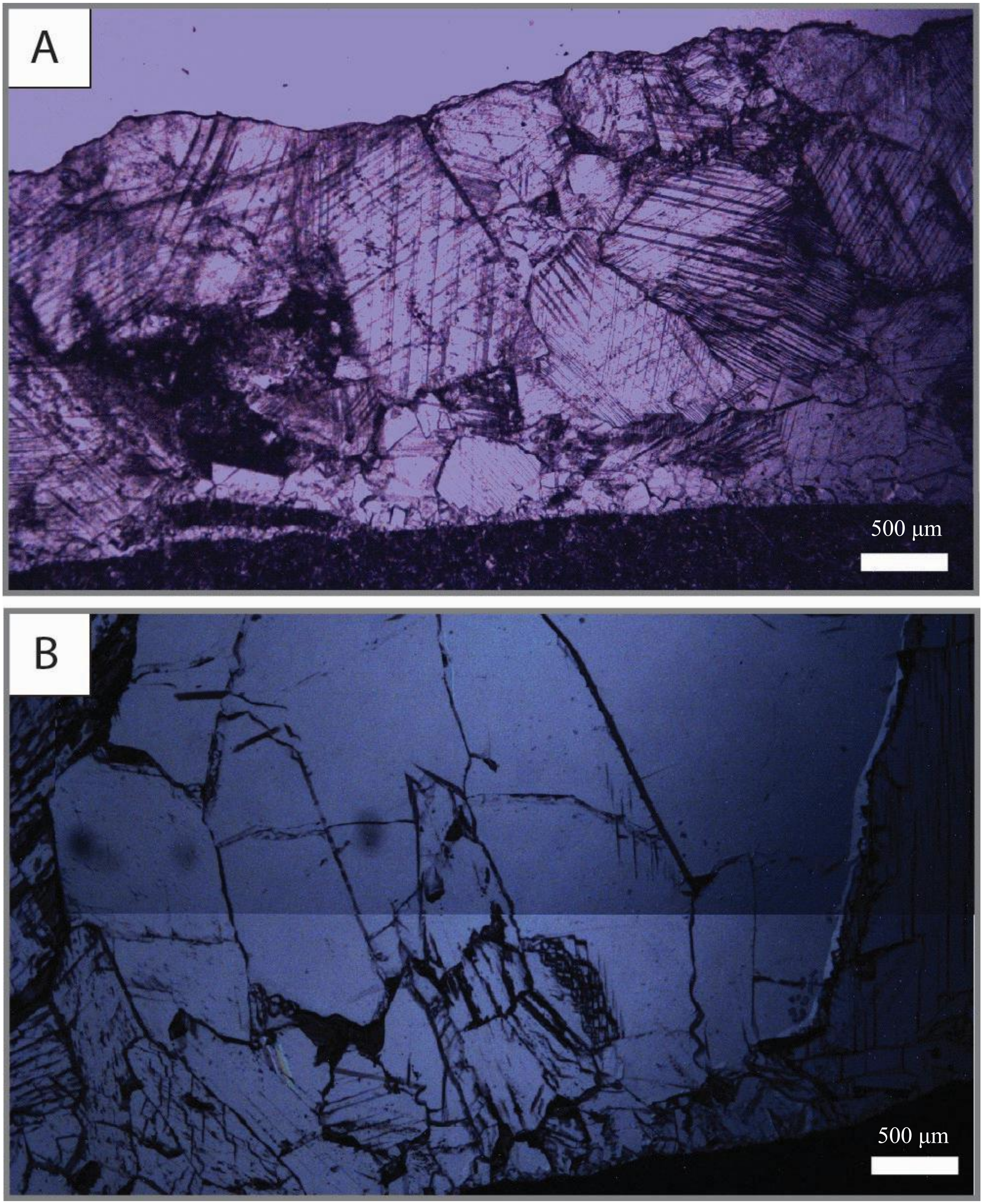

Figure 5: (A) is a calcite extension vein associated with NE-SW shortening (EV1). (B) is a calcite extension vein associated with the Washita Valley Fault System (EV3). Note that (A) exhibits a higher density of twinning relative to (B).

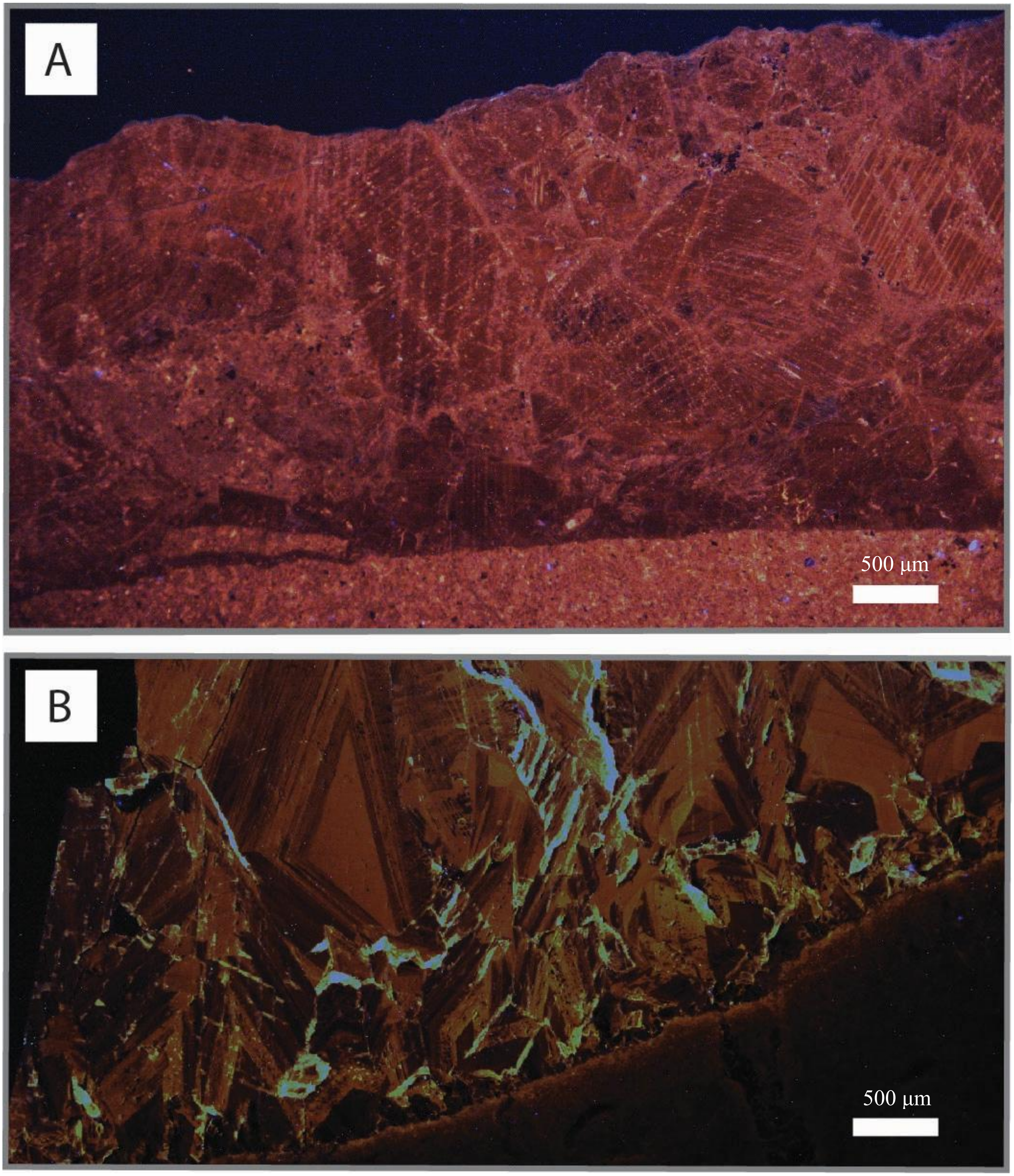

Figure 6: Cathodoluminescence images of extension veins related to NE-SW shortening (A) and the Washita Valley Fault System (B). These images were used for the selection of spot points for LA-ICP-MS.

4.3 U-Pb Calcite Ages

Six U-Pb ages were retrieved from syn-tectonic calcite, two related to NE-SW shortening (one flexural slip vein and one extension vein), and four related to the Washita Valley Fault System (three extension veins and one slickenfiber) (Figures 7 & 8). Spot points from a selected thin section were not included within the age calculation under the following parameters: the spot point intersected a sulfide or fluid inclusion, the spot point intersected grain boundaries, zonation boundaries, or fractures, the spot point showed an error ≥ 20% (2σ-sigma error) and is discordant with the lower intercept, or if the spot point lies within host rock matrix. Host rock matrix was ablated with veins separately to provide a comparison in the case of host rock inclusion.

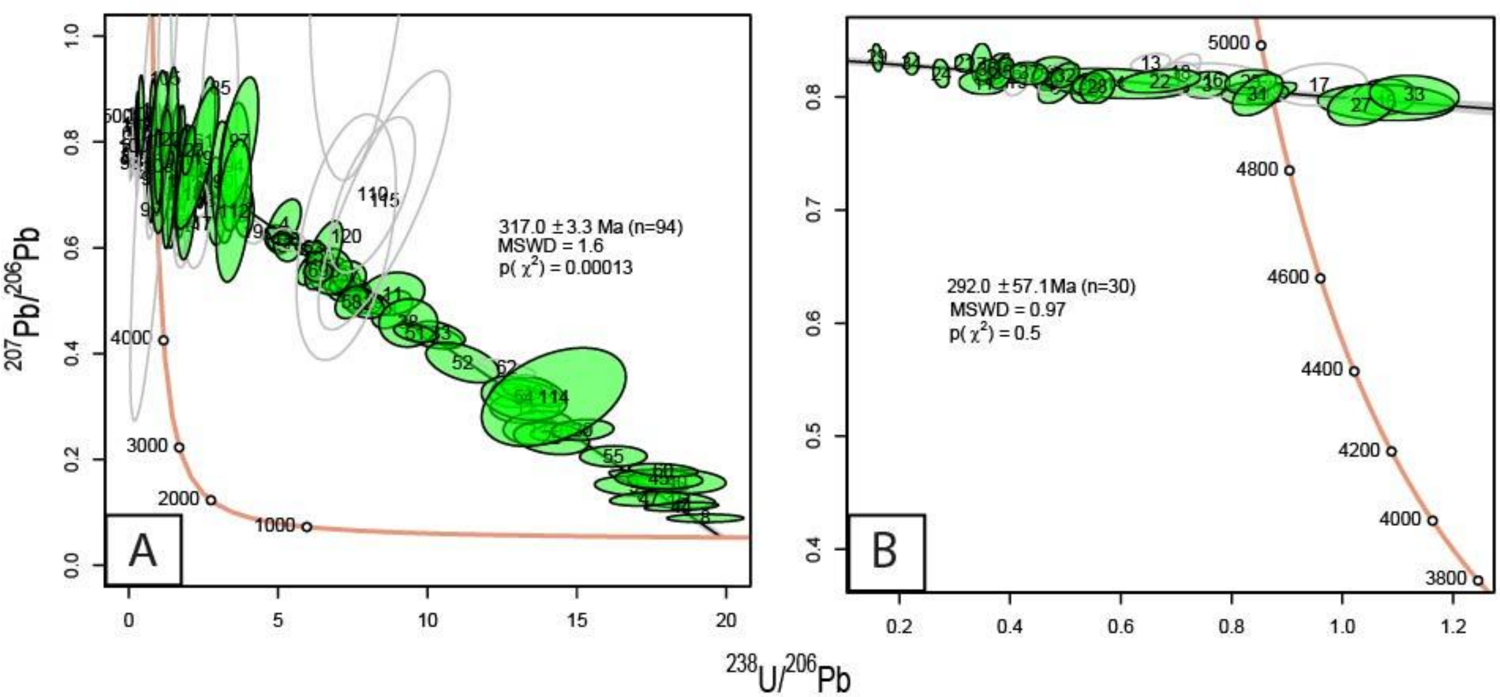

Figure 7: U-Pb ages derived from syn-tectonic veins associated with NE-SW shortening.

The dates associated with NE-SW shortening ranged from 292 ± 57 Ma to 317 ± 3.3 Ma (2σ-sigma error) (Figure 7). The younger age was derived from a flexural slip vein and showed an error much higher than its extension vein counterpart due to the high measurements of common Pb in the system. The four ages associated with the Washita Valley Fault System were derived from three extension veins (A, C, & D in Figure 8) and one slickenfiber (B in Figure 8). These ages exhibit an age range between 144.3 ± 22.9 Ma and 109.5 ± 3.8 Ma (2σ-sigma error) (Figure 8). Three of the four of these ages contain high amounts of radiogenic Pb, which lead to more accurate ages.

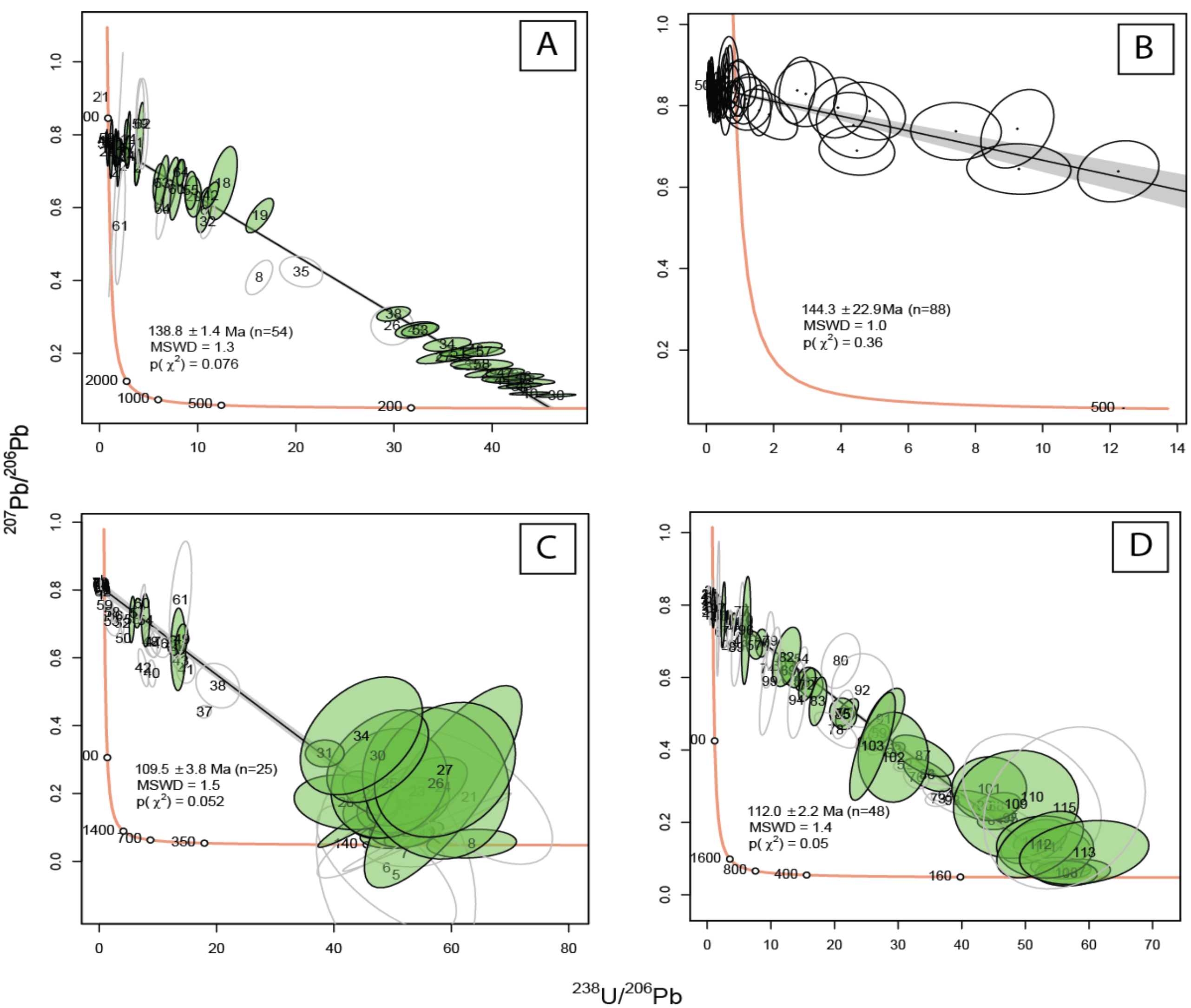

Figure 8: U-Pb ages derived from syn-tectonic Washita Valley Fault System extension veins (A, C, D) and shear veins (B).

4.4 Stable Isotopes

4.4.1 Conventional Isotopes O and C

Carbon and Oxygen isotope composition of collected calcite veins (EV3 and SV3) and their respective host rock (HR) are presented in Table 1. $\delta^{18}O_{VPDB}$ and $\delta^{13}C_{VPDB}$ values of Washita Valley Fault System veins range from -6.61 ‰ to -3.69 ‰ and from– 6.51 ‰ to +1.66 ‰, respectively. Their host rock ranges from – 0.57 ‰ to +0.96 ‰ for $\delta^{13}C_{VPDB}$ and from -3.69 ‰ -10.35 ‰ for $\delta^{18}O_{VPDB}$ (Figure 9). Low ^{18}O and moderate $\delta^{13}C$ values of extension vein host rock is reflective of pre-Carboniferous marine carbonates reported by Gao et al. (1993) and Upper Cambrian-Lower Ordovician stratal dolomites from the Arbuckle Group reported by Gao & Eldmore (1995) (Figure 9). On analyzed samples, vein/host rock pairs systematically show different $\delta^{18}O$ values. Such differences usually reflect oxygen isotopic disequilibrium between the fluid and the host rocks during vein opening.

Sample	$\delta^{13}C$ VPDB	std.dev.	$\delta^{18}O$ VPDB Calcite	$\delta^{18}O$ VSMOW Calcite	std.dev.	Yield% (as CaCO3)
ARB23-05-2-HR	0.07	0.03	-4.48	26.30	0.03	34.9
ARB23-05-3-EV3	-4.20	0.09	-3.69	27.11	0.09	113.3
ARB23-05-4-EV3	-0.16	0.06	-5.05	25.70	0.05	105.7
ARB23-06-1-HR	0.96	0.07	-3.69	27.10	0.07	71.0
ARB23-06-2-HR	-0.36	0.07	-3.92	26.87	0.07	70.0
ARB23-06-3-EV3	1.66	0.11	-4.84	25.92	0.10	98.0
ARB23-06-4-EV3	1.41	0.12	-5.99	24.73	0.11	95.6
ARB19-07-1-HR	-0.57	0.03	-10.35	20.24	0.07	21.0
ARB19-07-2-EV3	-6.51	0.07	-6.61	24.09	0.07	113.6

Table 1: Isotopic compositions ($\delta^{18}O$ and $\delta^{13}C$, ‰) of carbonate host rock samples and extension veins from the Washita Valley Fault System.

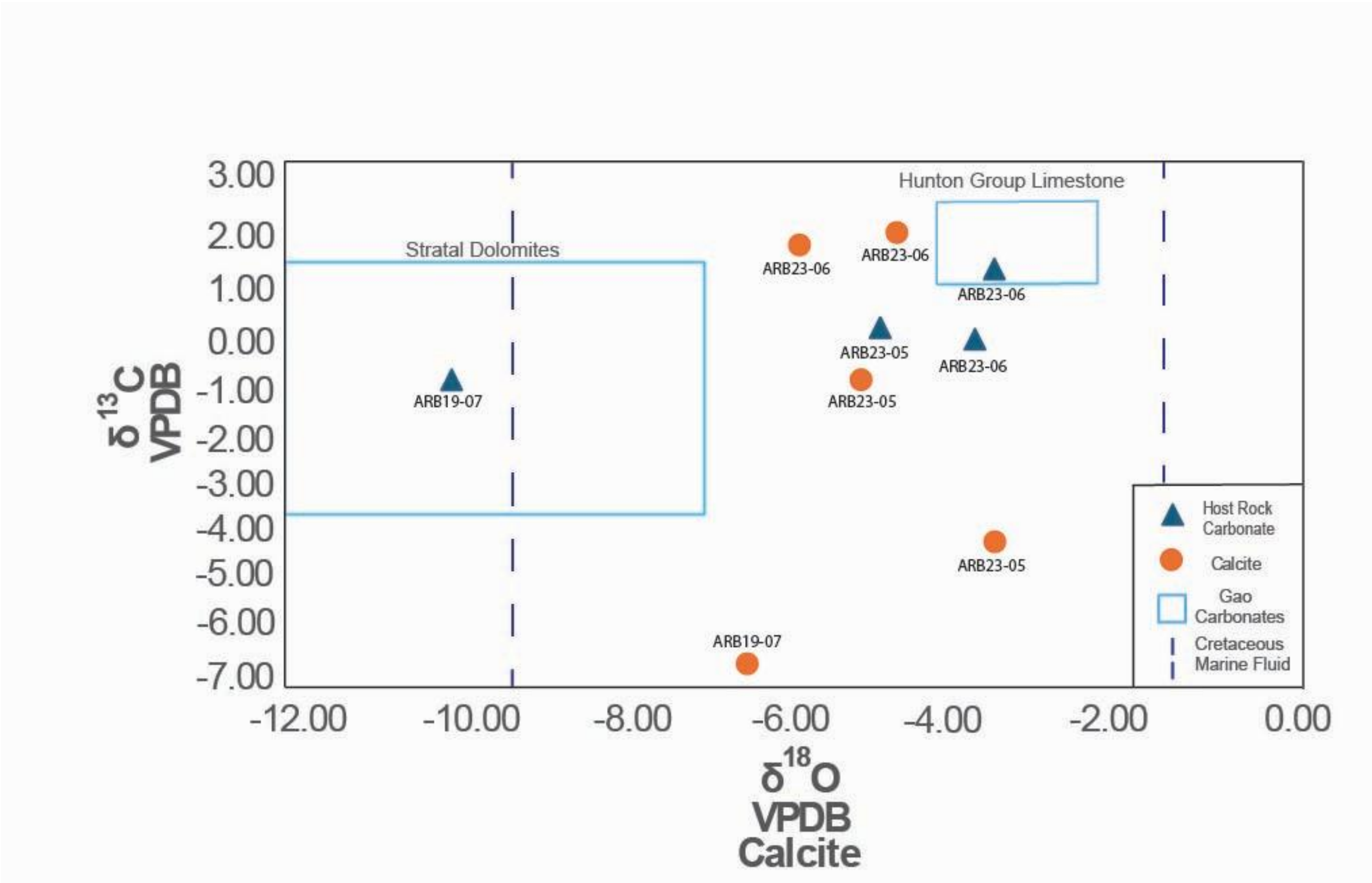

Figure 9: Isotopic compositions ($\delta^{18}O$ and $\delta^{13}C$, ‰) of carbonate host rock and veins from the Washita Valley Fault System alongside $\delta^{18}O$ and $\delta^{13}C$, ‰ compositions of host stratigraphy from Gao (1990), Gao & Land (1991), Gao et al. (1993) and Gao & Eldmore (1995). Dashed lines represent a combination of $\delta^{18}O_{Seawater}$ composition ranges of marine fossils from the Western Interior Seaway (Coulson & Barrick 2011, Taylor et al. 2021).

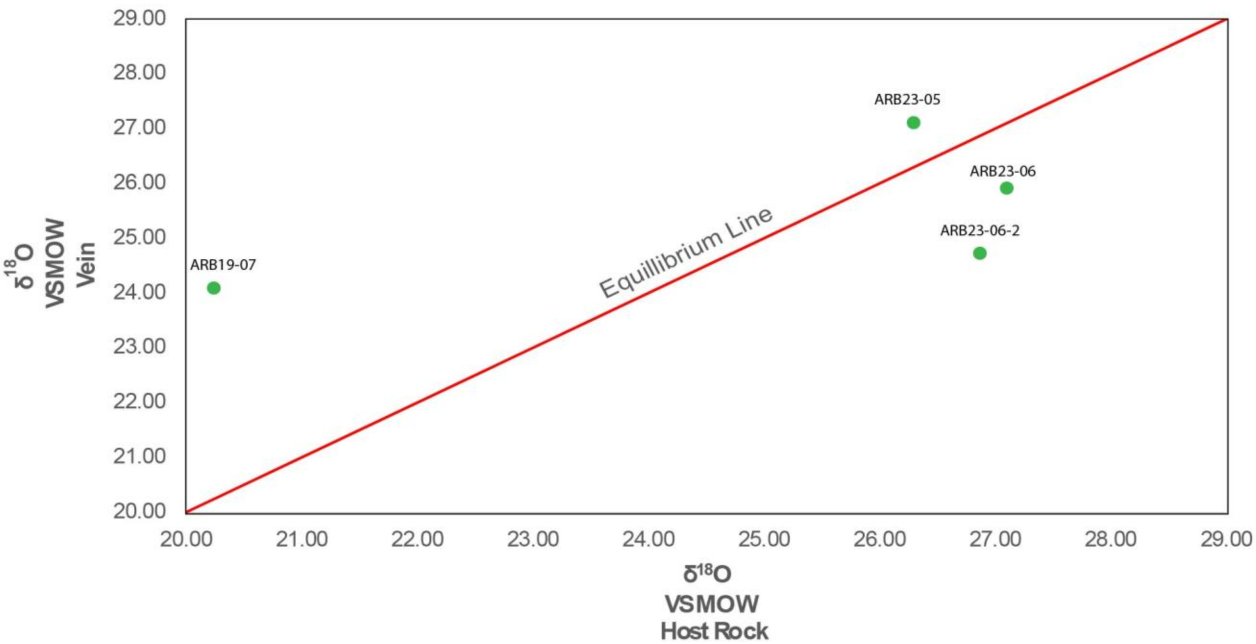

Figure 10: $\delta^{18}O$ compositions of extension veins and their host rocks. Note vein samples are not in equilibrium with their host rocks indicative of buffering.

Sample	Category	$\delta^{13}C$ VPDB	$\delta^{18}O$ VPDB Calcite	$\delta^{18}O$ VSMOW Calcite	$\Delta_{47\text{-}90}$ ETF-Cc	T-3 (Anderson et al, 2021)	$\delta^{18}O$ VSMOW Fluid (Zheng)	n
ARB19-07-1	Extension Vein	-5.69	-6.73	23.98	0.542	44.5	-0.6	2
ARB19-07-2	Extension Vein	-6.17	-6.67	24.04	0.546	44	-6.67	2
ARB21-1B-1	Slickenfibre	-4.74	-6.75	23.95	0.499	64	1.42	2
ARB21-1B-2	Slickenfibre	-4.83	-6.84	23.86	0.490	68	3.60	2
ARB23-05-4	Extension Vein	0.03	-5.35	25.40	0.530	45	-1.92	2
ARB23-06-3	Extension Vein	1.74	-5.34	25.40	0.533	44	-2.06	2

Table 2: Results from Δ_{47} clumped isotope analysis.

4.4.2 Δ_{47} Clumped Isotope Analysis

Δ_{47} clumped-isotope composition of extension veins and slickenfibers associated with the Washita Valley Fault System have been measured to refine the temperature of calcite precipitation as well as to determine the $\delta^{18}O$ compositions of the mineralizing fluid. Based on two replicates, the Δ_{47} compositions from extension veins range between 0.530 and 0.546 ‰, and slickenfibers range between 0.490 and 0.499 ‰ (Table 2). Temperatures of the mineralizing fluid were determined by applying the calibration from Anderson et al. (2021) (Equation 2). TΔ47 range between 44 to 45 °C for Extension vein (EV3, and from 64 to 68 °C for slickenfibers (SV3). This suggest that syn-tectonic veins reflecting Washita Valley Fault System activity formed at temperature between 44 and 68 °C (Figure 10).

The oxygen isotopic compositions of the fluid involved during the Washita Valley Fault activity were determined using the oxygen isotope fractionation factor of O'Neil et al. (1969) and Zheng (1998), the $\delta^{18}O_{VSMOW}$ of calcite and TΔ47 (Figure 10). These isotopic compositions as well as those produced from conventional methods were plotted alongside Δ_{47} temperatures. The oxygen isotope composition of the mineralizing fluid involved during the Washita Valley Fault activity varies from -2.06 and 3.60‰ VSMOW. Such $\delta^{18}O$ compositions reflect marine fluid composition with a potential supplement of meteoric fluid when paired with the Δ_{47} temperatures (Figure 11).

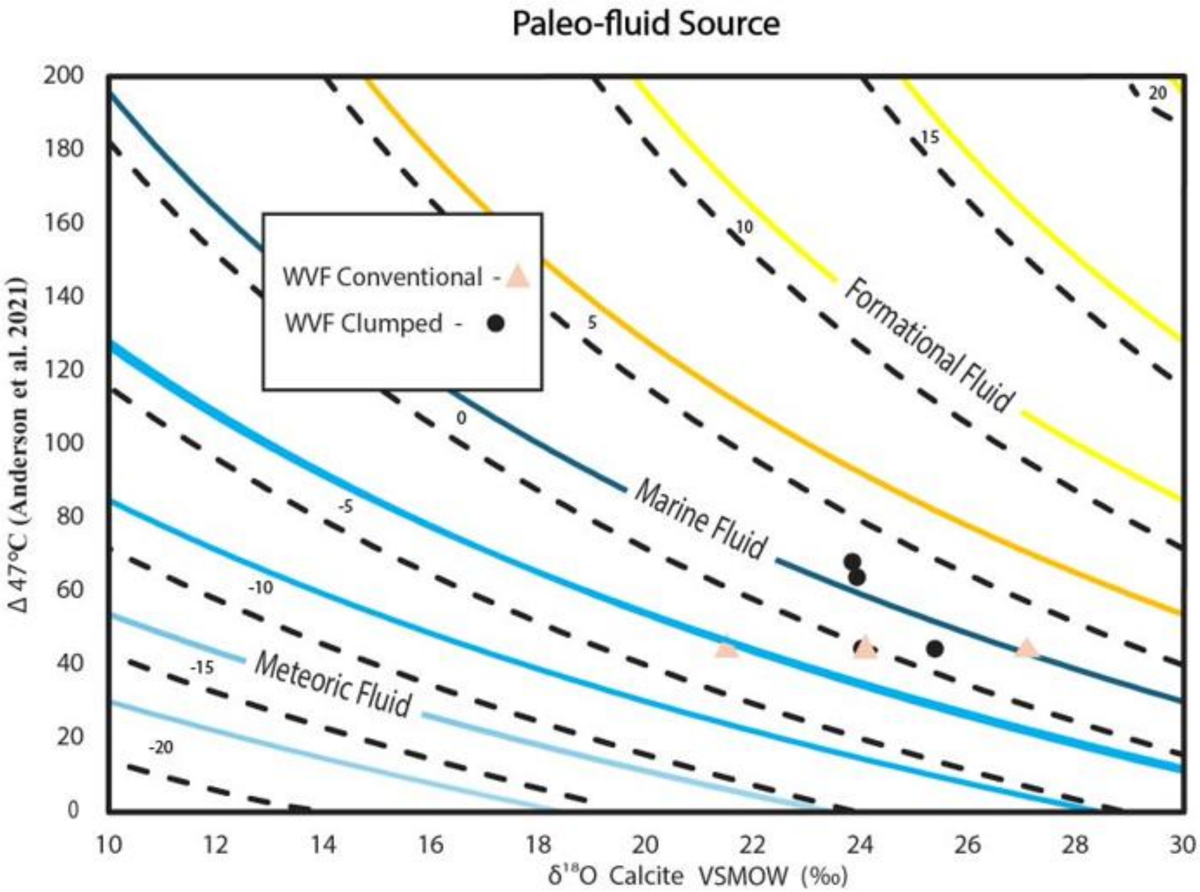

Figure 11: Temperature (°C) vs. $\delta^{18}O_{VSMOW}$ of calcite. Dashed and plain lines correspond to the $\delta^{18}O$ composition of the mineralizing fluid calculated using the oxygen fractionation equations from O'Neil et al. (1969) (plain lines) and Zheng (1998) (dashed lines). Temperatures for the mineralizing fluids of syn-tectonic calcite are identified using Δ_{47} clumped isotope analysis.

Chapter 5 - Discussion

The purpose of this study is to better constrain the timing and activity conditions of the Washita Valley Fault System by combining detailed structural analysis at macro- and microscopic scale, petrography and isotope geochemistry. Such an approach has been commonly used to assess geochronological constraints and the temperature, pressure and origin of the mineralizing fluids within fault systems as well as to establish a geodynamic setting responsible for fault reactivation (e.g. Lacroix et al., 2014; Hoareau et al., 2021; Beaudoin et al., 2022; Roberts et al., 2022; Betania Palacios-García, 2023).

5.1 Geochronological Constraints

Based on seismic data interpretation across the Arbuckle Mountains, Turko (2019) and Turko and Tapp (2021) propose that the Washita Valley Fault System formed by the reactivation of a series of normal faults from the basement inherited from Southern Oklahoma Aulacogen during the Pennsylvanian. As the stress field responsible for the Arbuckle Orogeny rotated to an oblique position, with a horizontal stress oriented WNW-ESE, these authors suggest that the last stages of the Arbuckle Orogeny favored sinistral strike-slip displacement.

However, a strictly Pennsylvanian emplacement of the Washita Valley Fault System can be ruled out by several observations. First, both absolute and relative geochronological methods reflect an age range much younger than the Pennsylvanian for the Washita Valley Fault System. WNW-ESE sinistral faults belonging to the WVF system oriented have been observed within the Pennsylvanian Collins Ranch Conglomerate, post-Pennsylvanian sediments, and documented by regional mapping efforts (Ham, 1950; Carter, 1979; VanArsdale, 1989; Fay, 1989; Allen, 2000). Secondly, at micro-scale, D_3-related veins do not display significant calcite twins. In contrast, calcite cement from Pennsylvanian D_1-related veins is affected by a larger twinning density

(Type 1 twin). Because the density and the thickness of calcite twinning in calcite veins depends on the amount of stress accumulated, variability in calcite twinning density can be used as an indicator of stress history and relative timing (e.g., calcite crystals with higher densities of twinning indicate older ages) (Burkhard 1993; Ferrill et al., 2004; Lacombe et al. 2021). As such, D_1 veins are more densely twinned than D_3 veins indicating that D_1 veins have been exposed to more stress over their lifetime (Figure 5). These observations provide indirect evidence for a post Arbuckle Orogeny activity of the Washita Valley Fault System (Figure 12). Finally, the U/Pb ages from Washita Valley Fault System veins obtained in this study (Figure 8) reflect two much younger Cretaceous age ranges; 144.3 -138.8 Ma and 112 - 109.5 Ma.

These new data provide two potential implications for the revision of geochronology regarding the Washita Valley Fault System activity: 1) The Washita Valley Fault System remains interpreted as Pennsylvanian in age with at least two phases of reactivation during the Cretaceous, and 2) the age data suggests that the main activity of the Washita Valley Fault System was Cretaceous and not Pennsylvanian.

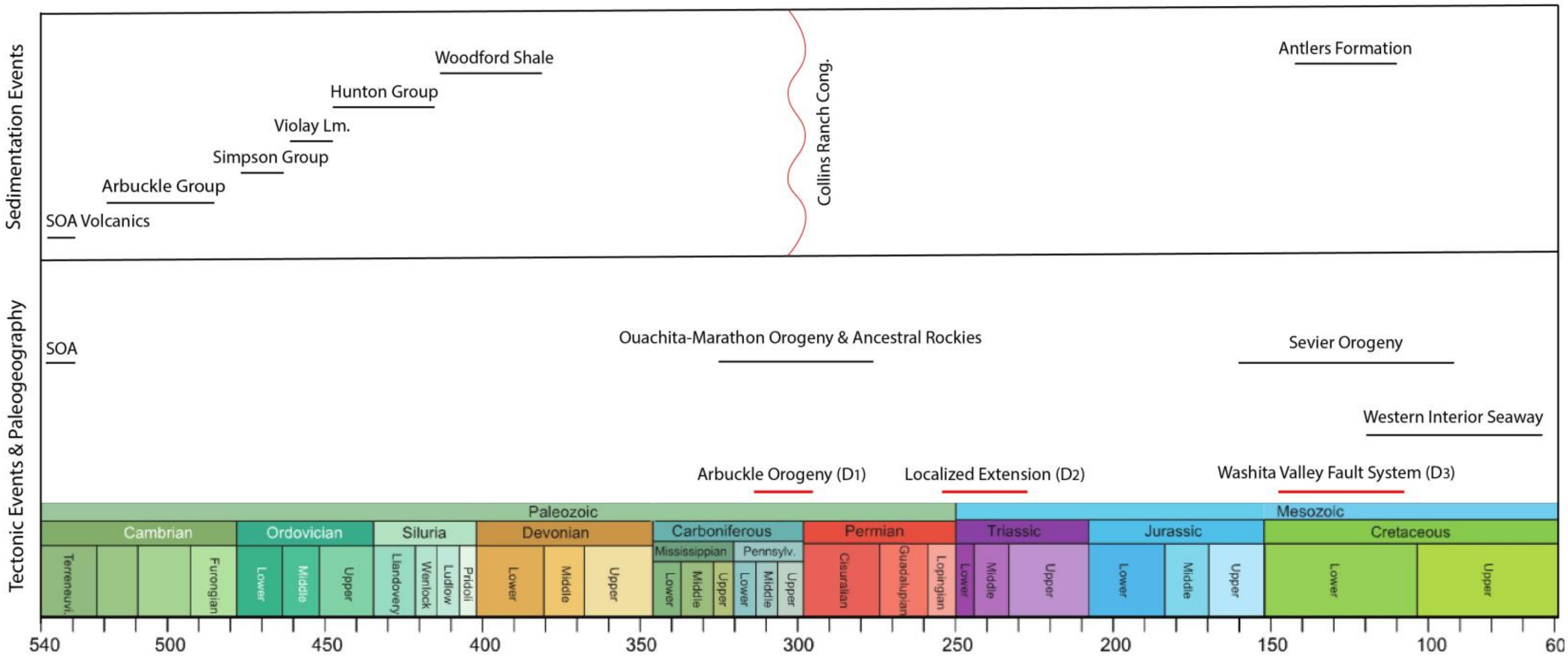

Figure 12: Timescale for the Arbuckle Mountain region starting with the Southern Oklahoma Aulacogen (SOA). Ages for individual events are provided for comparison to the Washita Valley Fault System (Ham, 1954; Fay, 1989; Kluth & Coney, 1981; Kluth, 1986; Budnik, 1986; Thomas, 1991; Poole, 2005; Keller, 2007; Slattery et al. 2013; Giallorenzo et al. 2017; Leary, 2017, Turko & Tapp 2020).

5.2 Mineralizing Fluids

Oxygen and carbon stable isotopic results suggest that syn-tectonic calcite veins from the Washita Valley Fault System are not in isotopic equilibrium with their host rock carbonates (Figure 10). Such isotopic disequilibrium indicates a low fluid-rock interaction during fault activity with a lack of buffering of the fluid by the surrounding host carbonate. Such conditions are typical from open paleo-hydrogeological system involving the contribution of an external fluid source (e.g., Lacroix et al., 2014; Beaudoin et al., 2022). In addition, the δ^{13}C depletion of calcite veins compared to their relative host rocks may indicate the contribution of organically derived carbon before calcite precipitation (e.g., Smeraglia et al., 2020).

The δ^{18}O compositions of mineralizing fluid from which both EV3 and SV3 precipitated from, range from -2.06 and 3.60‰ VSMOW, with an average of 0.26‰ VSMOW (Table 2 & Figure 11). Such fluid oxygen composition range is typical from marine and meteoric water during the

Cretaceous (Veizer & Prokoph, 2015) (Figure 9). Interestingly, the calculated $\delta^{18}O$ of mineralizing fluid falls within the $\delta^{18}O$ range of seawater from the Western Interior Seaway (Figure 9) determined via Cretaceous marine fossils (Coulson & Barrick 2011; Goedert et al. 2020; Taylor et al. 2021). This is in line with the palaeogeographical reconstruction of the Arbuckle Mountain region during Cretaceous which suggest that the studied area was covered by the Western Interior Seaway during Cretaceous (Kauffman 1985; Kauffman & Caldwell 1993; Roberts & Kirschbaum 1995; Slattery et al. 2013). The calculated $\delta^{18}O$ of mineralizing fluid also reflects a meteoric fluid component (Figure 11), consistent with near surface activity of the Washita Valley Fault. The shallow conditions of the fault activity are representative of an open hydrological system with incursion at depth and/or meteoric water. Formation and precipitation of veins require fluid pressure which is affected by host rock characteristics such as low permeability, previous fracturation, and increasing crustal depth (Bons et al. 2012). As pressure increases, openings occur, decreasing the pressure and allowing fluid infiltration (Bons et al 2012). A near surface, open hydrogeological system would prevent fluid pressure build-up, which provides evidence for why Washita Valley Fault System faults rarely display slickenfibers along their fault planes. The Washita Valley Fault System would then act as a conduit for marine fluids and/or provide a pathway for groundwater/marine fluid mixing into the subsurface.

5.3 Geodynamic Implications

Interestingly, the proposed revised age of the Washita Valley Fault System activity overlaps the current geochronological constraints of the Cretaceous initiation of the Sevier Orogeny to the west (Figure 12) (Giallorenzo et al. 2017; Malone et al. 2022). The Sevier Orogeny mainly formed from an E-W oriented primary stress associated with the subduction of the Farallon Plate under Western North America (Yonkee & Weil 2016; Giallorenzo et al. 2017;

Malone et al. 2022). Such maximum horizontal stress direction is consistent with the E-W primary stress orientation of the Washita Valley Fault System deduced from our detailed structural analysis (Figure 4). We suggest that the initiation/reactivation of the Washita Valley Fault System may have been produced by the far field stress of the Sevier Orogeny. With such more favorable orientation, the early stage of the Sevier Orogeny may require less stress to reactivate Washita Valley strike-slip faults along steeply dipping bedding planes from the north limb of the Arbuckle Anticline than forming thrust nappe stacking (Figure 13). In addition, the episodic nature of the Sevier fold-and-thrust belt described by Malone et al. (2022) provides the potential for the initiation/reactivation of the Washita Valley Fault System further to the east of the Sevier Orogeny.

With the proposed constraints on the absolute timing of the Washita Valley Fault System, the tectonic evolution of the Arbuckle Mountains can be refined into four distinct phases (Figure 13). 1) The Southern Oklahoma Aulacogen rifting phase ultimately led to the closure of the Rheic and Paleo-Tethys oceans and the collision of the Gondwana and Laurentia supercontinents (Kluth & Coney 1981; Kluth 1986; Budnik 1986; Thomas 1991; Poole, 2005; Keller 2007; Keller 2014; Leary 2017, Turko & Tapp 2021). 2) This collision causes an inversion of the Southern Oklahoma Aulacogen structures and marks the beginning of the Pennsylvanian Arbuckle Orogeny features (EV_1, $Styl_1$, and subsequent thrusting). 3) The localized Triassic normal faulting may result from the late phase of the opening of the Gulf of Mexico (Lacroix et al., 2022; Rickert et al., 2023, Curry 2024). 4) Shallow depth sinistral strike-slip faulting and associated features occur (EV_3 and $Styl_3$) during the Cretaceous. These faults trend E-W with larger densities of these faults present along steeply dipping bedding planes, consequently offsetting the fold axis of the Arbuckle Anticline (Tanner, 1967; Carter, 1979; Webster, 1980; Booth 1982; Brown and Grayson, 1985).

Southwestern Oklahoma is also home to several other large fault systems with similar NW-SE orientations as the Washita Valley Fault System such as the Cement Fault, Mountain View Fault, Meers Fault, Reagan Fault, Waurika-Muenster Fault, among others (Figure 14). It is widely accepted that the majority of these fault systems originated in the Pennsylvanian and are correlated with orogenic pulses which occurred in the Southern Oklahoma Aulacogen region (Wichita Mountain Uplift[s] and Arbuckle Uplift) (Jacobsen, 1949; Jacobson, 1984; Reed, 1959; Herrmann, 1961; Granath, 1989; Blome et al., 2014; George 2016; Turko 2019; Turko & Tapp 2021; Hobbs et al., 2022). However, post-Pennsylvanian deformation within these fault systems has been recorded for the Meers Fault in the Holocene (Madole, 1988), the Mountain View Fault in the Permian (Nielson & Stern 1985), and now the Washita Valley Fault System in the Cretaceous (this study). Our study provides an impetus for the further study of these large fault zones using isotope assisted structural geology to better constrain reactivation potential, geochronology, fluid history, and effects on the Anadarko Basin oil field within the Southern Oklahoma Aulacogen region. Furthermore, it is likely that these other, spatially aligned fault systems, may have also undergone phases of Mesozoic deformation like what we document here for the Washita Valley Fault system.

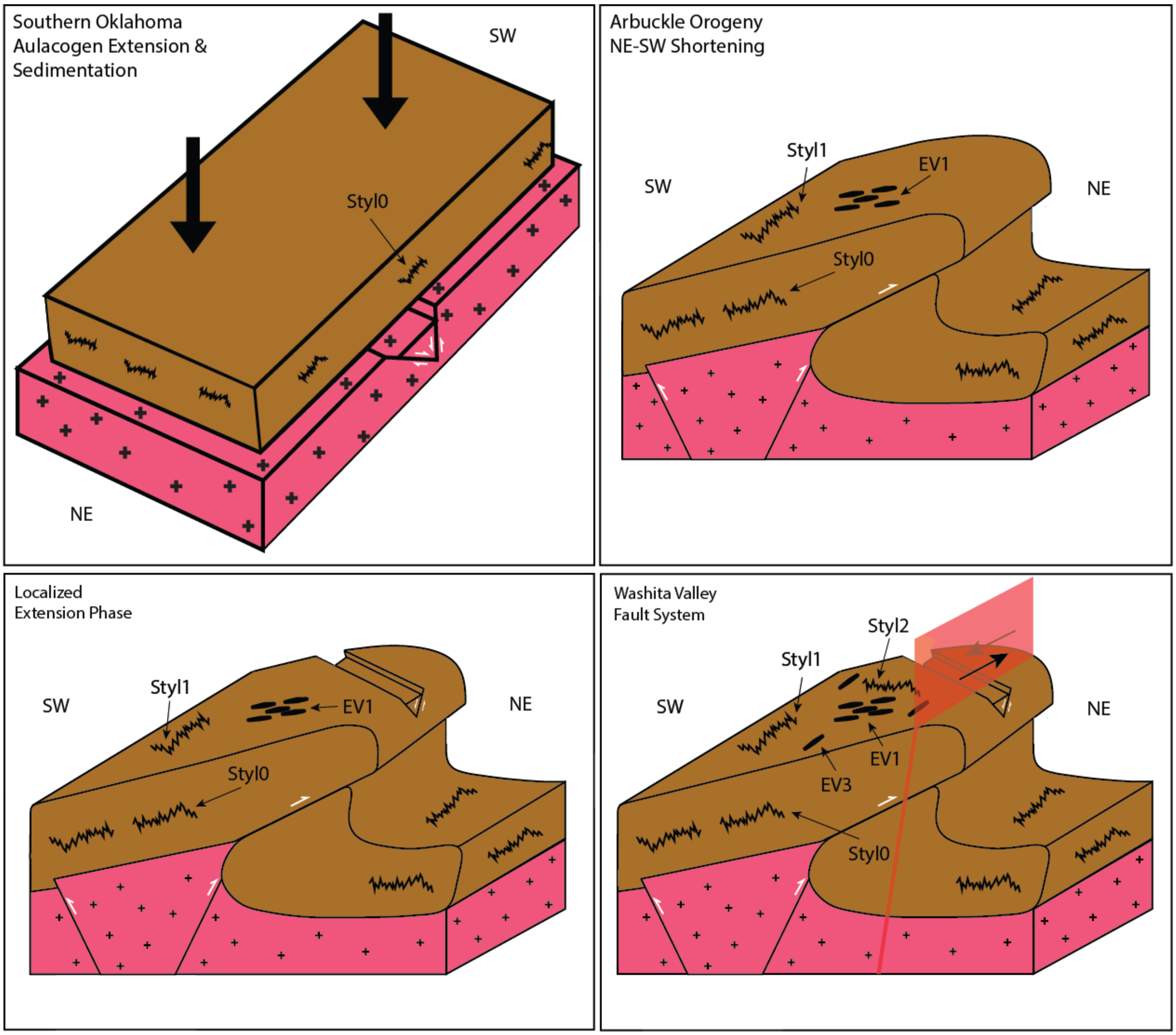

Figure 13: Block diagram illustrating the tectonic evolution of the Arbuckle Mountains given the age constraints acquired through structural observations and U-Pb geochronology.

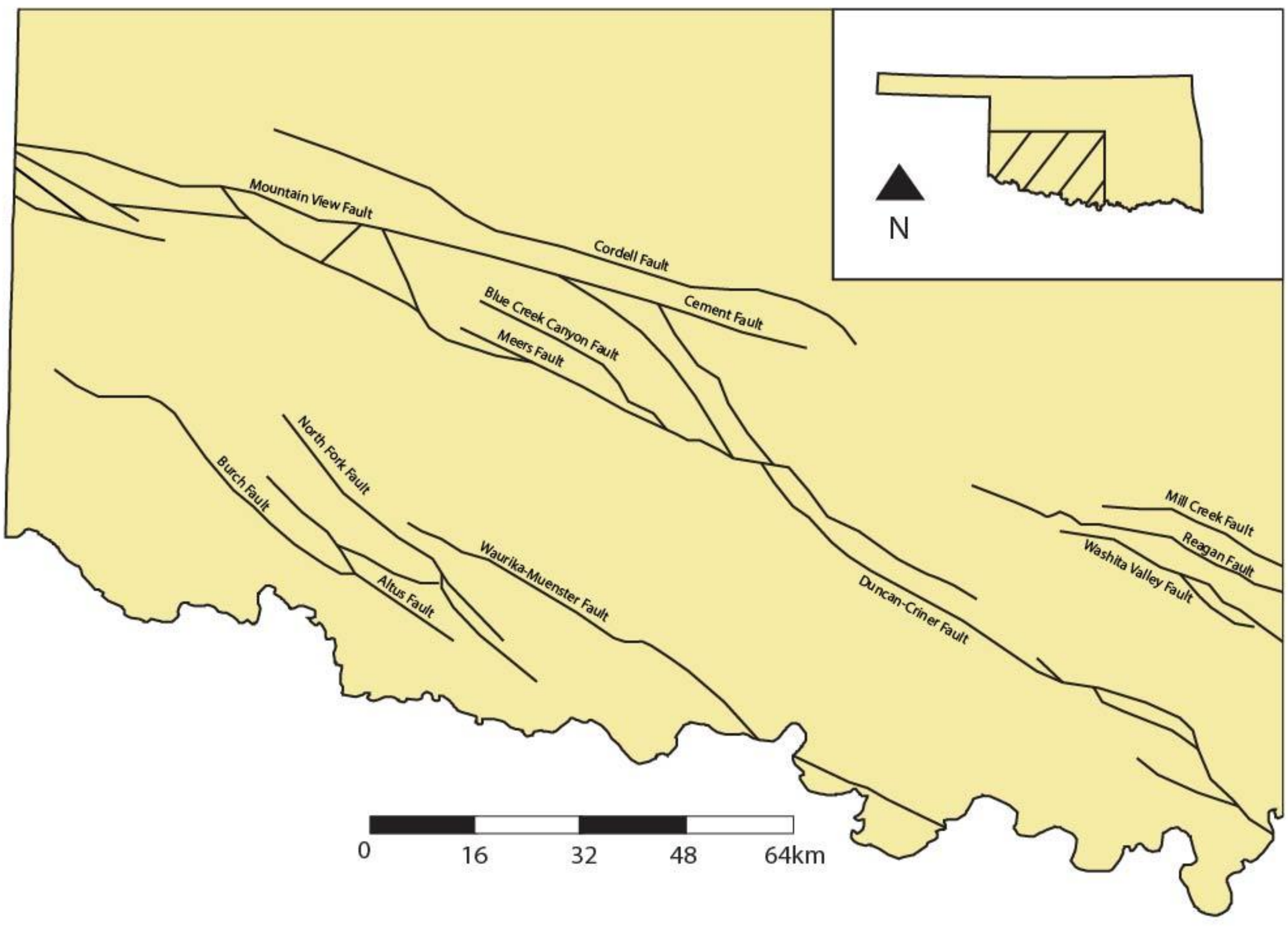

Figure 14: WNW-ESE oriented fault systems in southwestern Oklahoma. Map modified from Luza et al. (1987).

Chapter 6 - Conclusion

The new data produced in this study suggests that when combined, structural analysis, U-Pb geochronology, and Δ47 clumped isotope thermometry can provide an effective story on the tectonic evolution of fault systems. In total, 4 samples of syn-tectonic calcite vein cements related to the Washita Valley Fault System were dated and provided two distinct Cretaceous age ranges (144.3-138.8 Ma & 112-109.5 Ma). Two models can be derived from the age data. 1) The Washita Valley Fault System remains interpreted as Pennsylvanian in age with at least two phases of reactivation during the Cretaceous, and 2) the age data suggests that the main activity of the Washita Valley Fault System was Cretaceous and not Pennsylvanian. The E-W primary stress associated with the Sevier Orogeny is similar to that of in the Washita Valley Fault System in the Cretaceous. This E-W stress could likely be a source for the initiation/reactivation of the Washita Valley Fault System.

Oxygen isotopic composition and temperature of calcite precipitation were determined via conventional and Δ47 clumped stable isotope methods. These data reflect a $\delta^{18}O_{VSMOW}$ value of the syn-tectonic mineralizing fluid ranging from -2.06 and 3.60‰ VSMOW, and a temperature range of 44 to 68 °C. Such values and temperatures are consistent with marine fluid with a component of meteoric fluid for the composition of the mineralizing fluid. This fluid composition can be correlated to the marine fluid composition of the Western Interior Seaway in the Cretaceous. The Washita Valley Fault System would then act as a near surface conduit for marine and meteoric groundwater mixing.

The Washita Valley Fault System belongs to a series of NW-SE oriented fault systems in Oklahoma. Using the combination of structural analysis, U-Pb geochronology, and conventional as well as Δ47 clumped isotope thermometry, these other fault systems may reveal similar reactivated phases, hydrocarbon reservoir implications, fluid history, and geochronological histories.

References

Allen, R.W., 2000, Complex structural features of the Ardmore Basin: Shale Shaker Journal, 51,11–21.

Anderson, N. T., Kelson, J. R., Kele, S., Daëron, M., Bonifacie, M., Horita, J., et al. (2021). A unified clumped isotope thermometer calibration (0.5–1,100 °C) using carbonate-based standardization. Geophysical Research Letters, 48, e2020GL092069. https://doi.org/10.1029/2020GL092069

Badertscher, N.P., Beaudoin, G., Therrien, R., Burkhard, M., 2002. Glarus overthrust: a major pathway for the escape of fluids out of the Alpine orogen. Geology 30, 875e878.

Beaudoin NE, Lacombe O, Hoareau G, Callot J-P. How the geochemistry of syn-kinematic calcite cement depicts past fluid flow and assists structural interpretations: a review of concepts and applications in orogenic forelands. *Geological Magazine*. 2022;159(11-12):2157-2190. doi:10.1017/S0016756822001327

Bernasconi S.M., Daëron M., Bergmann K.D., Bonifacie M., Meckler A.N., Affek H.P., et al., 2021. InterCarb: A Community Effort to Improve Interlaboratory Standardization of the Carbonate Clumped Isotope Thermometer Using Carbonate Standards. Geochemistry, Geophysics, Geosystems, 22, e2020GC009588. https://doi.org/10.1029/2020GC009588.

Bernasconi S. M., Müller I. A., Bergmann K. D., Breitenbach S. F. M., Fernandez A., Hodell D. A., Jaggi M., Meckler A.N., Millan I. and Ziegler M., 2018. Reducing uncertainties in carbonate clumped isotope analysis through consistent carbonate-based standardization. Geochemistry, Geophysics, Geosystems, 19, 2895–2914. https://doi.org/10.1029/2017GC007385

Betania Palacios-García, N, Elisa Fitz-Díaz, Lisa D. Stockli, Daniel F. Stockli, *U–Pb calcite dating of brittle deformation in Permian carbonates within the Chicomuselo fold and thrust belt, SE Mexico*, Journal of Structural Geology, Volume 171, 2023, 104863, ISSN 0191-8141, https://doi.org/10.1016/j.jsg.2023.104863.

Blome, C. D., Golab, J. A., Lidke, D. J., & Wahl, R. R. (2014). Geologic Map of Chickasaw National Recreation Area, Murray County, Oklahoma with explanatory text (Map 3258, scale 1:24,000). U.S. Geological Survey Scientific Investigations. Retrieved from http://pubs.usgs.gov/sim/3258/

Boles, J.R., Eichhubl, P., Garven, G., Chen, J., 2004. Evolution of a hydrocarbon migration pathway along basin-bounding faults: evidence from fault cement. AAPG Bull. 88, 947e970.

Bonifacie, Magali, Damien Calmels, John M. Eiler, Juske Horita, Carine Chaduteau, Crisogono Vasconcelos, Pierre Agrinier, et al. 2017. "Calibration of the dolomite clumped isotope thermometer from 25 to 350°C, and implications for a universal calibration for all (Ca, Mg, Fe)CO3 carbonates." Geochimica et Cosmochimica Acta 200: 255-279.

Bons, P. D., Elburg, M. A., & Gomez-Rivas, E. (2012). *A review of the formation of tectonic veins and their microstructures. Journal of Structural Geology, 43, 33–62.* doi:10.1016/j.jsg.2012.07.005

Booth, S. L., 1982, Structural analysis of portions of the Washita Valley Fault zone, Arbuckle Mountains, Oklahoma: Shale Shaker Journal, 31, 107–120.

Brewer, J. A., COCORP Deep Seismic Reflection Traverse Across Southern Oklahoma Aulacogen: *AAPG Bulletin* 1981;; 65 (8): 1496. doi: https://doi.org/10.1306/03B5958A-16D1-11D7-8645000102C1865D

Brown, G.W., Grayson, R.C. Jr., Jamiesom, R. H. Jr., Altum, J. T., and Hightower, J., 1985, Tectonism and sedimentation in the Arbuckle Mountain region, southern Oklahoma aulacogen: Baylor Univ., Waco Texas, p. 1-6.

Brueseke, M. E., Hobbs, J. M., Bulen, C. L., Mertzman, S. A., Puckett, R. E., Walker, J. D., & Feldman, J. (2016). Cambrian intermediate-mafic magmatism along the Laurentian margin: Evidence for flood basalt volcanism from well cuttings in the Southern Oklahoma Aulacogen (U.S.A.). Lithos, 260, 164–177. doi:10.1016/j.lithos.2016.05.016

Budnik, R. T., 1986, Left-lateral intraplate deformation along the Ancestral Rocky Mountains: Implications for Late Paleozoic plate motions: Tectonophysics, 132,195–214, doi:10.1016/0040-1951(86)90032-6.

Burkhard, M. (1993). *Calcite twins, their geometry, appearance and significance as stress-strain markers and indicators of tectonic regime: a review. Journal of Structural Geology, 15(3-5), 351–368.* doi:10.1016/0191

Carter, D. W., 1979, A study of the strike-slip movement along the Washita Valley Fault, Arbuckle Mountains, Oklahoma: Shale Shaker Journal, 30, 85–115.

Chacko, T., Cole, D.R. and Horita, J. (2001) Equilibrium oxygen, hydrogen and carbon isotope fractionation factors applicable to geological systems. Reviews in Mineralogy and Geochemistry 43, 1-81.

Coulson, A. B., Kohn, M. J., & Barrick, R. E. (2011). *Isotopic evaluation of ocean circulation in the Late Cretaceous North American seaway. Nature Geoscience, 4(12), 852–855.* doi:10.1038/ngeo1312

Curry, M. E., Hudec, M. R., Peel, F. J., Fernandez, N., Apps, G., & Snedden, J. W. (2024). Structural restorations of the complete conjugate US-Mexico eastern Gulf of Mexico margin. *Tectonics*, 43, e2023TC007897. **https://doi.org/10.1029/2023TC007897**

David H. Malone, John P. Craddock, Alexandros Konstantinou*, 2022. "Timing and structural evolution of the Sevier thrust belt, western Wyoming", Tectonic Evolution of the Sevier-Laramide Hinterland, Thrust Belt, and Foreland, and Postorogenic Slab Rollback (180–20 Ma), John P. Craddock, David H. Malone, Brady Z. Foreman, Alexandros Konstantinou. https://doi.org/10.1130/2022.2555(04)

Dunham, R. J.,1955, Pennsylvanian conglomerates, structure, and orogenic history of the Lake Classen Area, Arbuckle Mountains, Oklahoma: AAPG Bulletin, 39,1–30, doi:10.1306/5CEAE0D9-16BB-11D7-8645000102C1865D.

Fay, O.R., 1989, Geology of the Arbuckle Mountains along Interstate 35, Carter and Murray Counties, Oklahoma: Oklahoma Geological Survey Guidebook 26, 50 p.

Ferrill, David A., Calcite twin widths and intensities as metamorphic indicators in natural low-temperature deformation of limestone, Journal of Structural Geology, Volume 13, Issue 6, 1991, Pages 667-675, ISSN 0191-8141, https://doi.org/10.1016/0191-8141(91)90029-I.

Ferrill, David A., Alan P. Morris, Mark A. Evans, Martin Burkhard, Richard H. Groshong, Charles M. Onasch, Calcite twin morphology: a low-temperature deformation geothermometer, Journal of Structural Geology, Volume 26, Issue 8, 2004, Pages 1521-1529, ISSN 0191-8141, https://doi.org/10.1016/j.jsg.2003.11.028.

Fitz-Diaz, E., Hudleston, P., Siebenaller, L., Kirschner, D., Camprubí, A., Tolson, G., Puig, T.P., 2011. Insights into fluid flow and water-rock interaction during deformation of carbonate sequences in the Mexican fold-thrust belt. J. Struct. Geol. 33, 1237e1253.

Gao, G. (1990). *Geochemical and isotopic constraints on the diagenetic history of a massive stratal, late Cambrian (Royer) dolomite, Lower Arbuckle Group, Slick Hills, SW Oklahoma, USA. Geochimica et Cosmochimica Acta, 54(7), 1979–1989.* doi:10.1016/0016-7037(90)90266-n

Gao, G. L. S. Land; Early Ordovician Cool Creek Dolomite, middle Arbuckle Group, Slick Hills, SW Oklahoma, U.S.A.; origin and modification. *Journal of Sedimentary Research* 1991; 61 (2): 161–173. doi: https://doi.org/10.1306/D42676BD-2B26-11D7-8648000102C1865D

Gao, G. The temperatures and oxygen-isotope composition of early Devonian oceans. *Nature* 361, 712–714 (1993). https://doi.org/10.1038/361712a0

Gao, G., L. S. Land, and R. D. Elmore. 1995. "Multiple episodes of dolomitization in the Arbuckle group, Arbuckle Moutains, South-Central Oklahoma: Field, petrographic, and geochemical evidence." Journal of Sedimentary Research A65 (2): 321-331.

George, M. C. (2016). The Muenster uplift of North Texas: The easternmost expression of the Pennsylvanian ancestral rockies, (Master's thesis, UTD Theses Dissertations). University of Texas at Dallas. Retrieved from http://hdl.handle.net/10735.1/5324

Ghosh, Prosenjit, Jess Askins, Hagit Affek, Brian Balta, Guo Weifu, Edwin A. Schauble, Dan Schrag, and John M. Eiler. 2006. "13C–18O bonds in carbonate minerals: A new kind of paleothermometer." Geochimica et Cosmochimica Acta 70: 1439-1456.

Giallorenzo, M. A., Wells, M. L., Yonkee, W. A., Stockli, D. F., & Wernicke, B. P. (2017). *Timing of exhumation, Wheeler Pass thrust sheet, southern Nevada and*

California: Late Jurassic to middle Cretaceous evolution of the southern Sevier fold-and-thrust belt. GSA Bulletin, 130(3-4), 558–579. doi:10.1130/b31777.1

Gilbert, M.C., and McConnell, D.A., 1991: Cambrian Basement Rocks and the Setting for Deposition of Late Cambrian Sediments in Western Oklahoma. Oklahoma Geologic Survey Circular 92, p. 109-117.

Goedert, J., Amiot, R., Berthet, D., Fourel, F., Simon, L., L´ ecuyer, C., 2020. Combined oxygen and sulphur isotope analysis—a new tool to unravel vertebrate (paleo)- ecology. Sci. Nat. 107, 1–9.

Goldstein, Robert H., Reynolds, James, 1994. "Fluid Inclusions and their Origin", Systematics of Fluid Inclusions in Diagenetic Minerals, https://doi.org/10.2110/scn.94.31.0005

Granath, J. W., 1989, Structural evolution of the Ardmore Basin, Oklahoma: Progressive deformation in the foreland of the Ouachita collision: Tectonics, 8, 1015–1036, doi: 10.1029/TC008i005p01015.

Ham, W.E.,1950, Geology and petrology of the Arbuckle Limestone in the southern Arbuckle Mountains: Ph.D. dissertation, Yale University.

Ham, W.E., 1954, Collings Ranch Conglomerate, Late Pennsylvanian, in the Arbuckle Mountains, Oklahoma: American Association of Petroleum Geologists Bulletin, v. 38, p. 2035-2045.

Ham, W.E., Denison, R.E., and Merritt, C.A., 1964, Basement Rocks and Structural Evolution of Southern Oklahoma: Oklahoma Geological Survey Bulletin 95, 302p.

Ham, W.E., et al., 1973, Regional Geology of the Arbuckle Mountains, Oklahoma: OGS Special Publication 73-3, 61 p

Hansman, R. J., Albert, R., Gerdes, A., & Ring, U. (2017). Absolute Ages of Multiple Generations of Brittle Structures by U-Pb Dating of Calcite Absolute ages of multiple generations of brittle structures by U – Pb dating of calcite. Geology, 46(3), 207–210. https://doi.org/10.1130/G39822.1

Herrmann, L. A. (1961). Structural geology of cement-chickasha area, Caddo and Grady counties, Oklahoma. AAPG Bulletin, 45(12), 1971–1993. https://doi.org/10.1306/BC74374B-16BE-11D7-8645000102C1865D

Hessert, J. M. (2016). A structural investigation of the Arbuckle Anticline related to the Appalachian-Ouachita Orogen, (Master’s thesis). Texas Tech University. Retrieved from http://hdl.handle.net/2346/67120

Hill, C. A., Polyak, V. J., Asmerom, Y., & P. Provencio, P. (2016). Constraints on a Late Cretaceous uplift, denudation, and incision of the Grand Canyon region, southwestern Colorado Plateau, USA, from U-Pb dating of lacustrine limestone. Tectonics, 35(4), 896–906. https://doi.org/10.1002/2016TC004166

Hoareau, G., Claverie, F., Pecheyran, C., Barbotin, G., Perk, M., Beaudoin, N. E., Lacroix, B., and Rasbury, E. T.: *The virtual spot approach: a simple method for image U-Pb carbonate geochronology by high-repetition rate LA-ICP-MS*, EGUsphere [preprint], https://doi.org/10.5194/egusphere-2024-2366, 2024.

Hoareau, G., Crognier, N., Lacroix, B., Aubourg, C., Roberts, N. M. W., Niemi, N., … Suárez Ruiz, I. (2021). *Combination of Δ47 and U-Pb dating in tectonic calcite veins unravel the last pulses related to the Pyrenean Shortening (Spain). Earth and Planetary Science Letters, 553, 116636.* doi:10.1016/j.epsl.2020.116636

Hobbs, N. F., van Wijk, J. W., Leary, R., & Axen, G. J. (2022). Late Paleozoic evolution of the Anadarko Basin: Implications for Laurentian tectonics and the assembly of Pangea. Tectonics, 41, e2021TC007197. https://doi.org/10.1029/2021TC007197

Jacobsen, L. (1949). Structural relations on east flank of Anadarko basin, Cleveland and McClain counties, Oklahoma. AAPG Bulletin, 33(5), 695–719. https://doi.org/10.1306/3D933D55-16B1-11D7-8645000102C1865D

Jacobson, M. I. (1984). The Harrisburg trough, Stephens County, Oklahoma: An update. In J. G. Borer (Ed.), *Technical proceedings of the 1981 American association of petroleum geologists mid-continent regional meeting* (pp. 127–137). Oklahoma City Geological Society.

Jochum, K. P., Weis, U., Stoll, B., Kuzmin, D., Yang, Q., Raczek, I., Jacob, D. E., Stracke, A., Birbaum, K., Frick, D. A., Günther, D., and Enzweiler, J. (2011). *Determination of Reference Values for NIST SRM 610–617 Glasses Following ISO Guidelines*. Geostandards and Geoanalytical Research, 35(4), 397–429. https://doi.org/10.1111/j.1751-908X.2011.00120.x

Kauffman, E. 1985. *"Cretaceous Evolution of the Western Interior Basin of the United States", Fine-Grained Deposits and Biofacies of the Cretaceous Western Interior Seaway: Evidence of Cyclic Sedimentary Processes*, Lisa M. Pratt, Erle G. Kauffman, Frederick B. Zelt

Keller, G.R., and Stephenson, R.A., 2007, *The Southern Oklahoma and Dniepr-Donets Aulacogens: A comparative analysis*, in Hatcher, R. D., Jr., Carlson, M. P., McBride, J.H., and Martínez Catalán, J.R., eds., The 4D Framework of Continental Crust: Geological Society of America Memoir 200, p. 127-143

Keller, G. R., 2014, *The Southern Oklahoma Aulacogen: It's a classic*, in N. H. Suneson, ed., Igneous and tectonic history of the Southern Oklahoma Aulacogen: Okla homa Geological Survey Guidebook, 38, 389–391.

Kim, S.-T. and O'Neil J.R., 1997. Equilibrium and non-equilibrium oxygen isotope effects in synthetic carbonates. Geochim. Cosmochim. Acta 61, 3461-3475.

Kim, S. T., Mucci, A., and Taylor, B. E. 2007. Phosphoric acid fractionation factors for calcite and aragonite between 25 and 75 °C: revisited. Chem. Geol. 246(3-4), 135–146.

Kluth, C. F., and P. J. Coney, 1981, *Plate tectonics of the Ancestral Rocky Mountains*: Geology, 9,10–15.

Kluth, C. F., 1986, *Plate tectonics of the Ancestral Rocky Mountains*, in J. A. Peterson, ed., Paleotectonics and sedimentation in the Rocky Mountains region, United States: AAPG Memoir, 41, 353–369.

Kauffman, E. & Caldwell, William. 1993. *The Western Interior Basin in space and time*. Geological Association of Canada Special Paper. 39.

Lacroix, B., Buatier, M., Labaume, P., Travé, A., Dubois, M., Charpentier, D., … Convert-Gaubier, D. (2011). *Microtectonic and geochemical characterization of thrusting in a foreland basin: Example of the South-Pyrenean orogenic wedge (Spain). Journal of Structural Geology, 33(9), 1359–1377.* doi:10.1016/j.jsg.2011.06.006

Lacroix, B., Travé, A., Buatier, M., Labaume, P., Vennemann, T., & Dubois, M. (2014). *Syntectonic fluid-flow along thrust faults: Example of the South-Pyrenean fold-and-thrust belt. Marine and Petroleum Geology, 49, 84–98.* doi:10.1016/j.marpetgeo.2013.09.005

Lacroix, B., Baumgartner, L. P., Bouvier, A.-S., Kempton, P. D., & Vennemann, T. (2018). *Multi fluid-flow record during episodic mode I opening: A microstructural and SIMS study (Cotiella Thrust Fault, Pyrenees). Earth and Planetary Science Letters, 503, 37–46.* doi:10.1016/j.epsl.2018.09.016

Lacroix, B., Bruce, H., Akers, M., Payne, J., and Moeller, A., "Refining Syn-Tectonic Diagenetic and Structural History of the Arbuckle Mountains", (2022) Geological Society of America Abstracts, vol. 54, Art. no. 383782. doi:10.1130/abs/2022AM-383782.

Lacombe, O.; Parlangeau, C.; Beaudoin, N.E.; Amrouch, K. *Calcite Twin Formation, Measurement and Use as Stress–Strain Indicators: A Review of Progress over the Last Decade. Geosciences* 2021, *11*, 445. doi:10.3390/2021gs11110445

Leary, R. J., P. Umhoefer, M. E. Smith, and N. Riggs, 2017, *A three-sided orogen: A new tectonic model for Ancestral Rocky Mountain uplift and basin development*: Geology, 45, 399–402, doi: 10.1130/G38830.1.

Luza, K. V., Madole, R. F., Crone, A. J., Oklahoma Univ., Norman (USA), & Nuclear Regulatory Commission, Washington, DC (USA). Div. of Engineering Research. (1987). *Investigation of the Meers fault in southwestern Oklahoma*.

Madole R. F. Stratigraphic evidence of Holocene faulting in the mid-continent: The Meers fault, southwestern Oklahoma. *GSA Bulletin* 1988;; 100 (3): 392–401. doi: https://doi.org/10.1130/0016-7606(1988)100<0392:SEOHFI>2.3.CO;2

Mangenot, X., Bonifacie, M., Gasparrini, M., Götz, A., Chaduteau, C., Ader, M., & Rouchon, V. (2017). *Coupling Δ 47 and fluid inclusion thermometry on carbonate cements to precisely reconstruct the temperature, salinity and δ 18 O of paleo-groundwater in sedimentary basins. Chemical Geology, 472, 44–57.* http://dx.doi.org/10.1016/j.chemgeo.2017.10.011

Mangenot, X., Gasparrini, M., Gerdes, A., Bonifacie, M., & Rouchon, V. (2018). *An emerging thermochronometer for carbonate-bearing rocks: Δ47 /(U-Pb). Geology, 46(12), 1067–1070.* doi:10.1130/g45196.1

Nielsen, K. C. & Stern R. J.; Post-Carboniferous tectonics in the Anadarko Basin, Oklahoma: Evidence from side-looking radar imagery. *Geology* 1985;; 13 (6): 409–412. doi: https://doi.org/10.1130/0091-7613(1985)13<409:PTITAB>2.0.CO;2

Nuriel, P., Weinberger, R., Kylander-Clark, A. R. C., Hacker, B. R., & Craddock, J. P. (2017). *The onset of the Dead Sea transform based on calcite age-strain analyses. Geology, 45(7), 587–590.* doi:10.1130/g38903.1

O'Neil, J. R., Clayton, R. N., & Mayeda, T. K. (1969). *Oxygen Isotope Fractionation in Divalent Metal Carbonates. The Journal of Chemical Physics, 51(12), 5547–5558.* doi:10.1063/1.1671982

Paton, C., Hellstrom, J., Paul, B., Woodhead, J., and Hergt, J. (2011). *Iolite: Freeware for the visualisation and processing of mass spectrometric data*. Journal of Analytical Atomic Spectrometry, 26(12), 2508–2518. https://doi.org/10.1039/C1JA10172B

Paton, C., Woodhead, J. D., Hellstrom, J. C., Hergt, J. M., Greig, A., and Maas, R. (2010). *Improved laser ablation U-Pb zircon geochronology through robust downhole fractionation correction*. Geochemistry, Geophysics, Geosystems, 11(3). https://doi.org/10.1029/2009GC002618

Petersen, S. V., Defliese, W. F., Saenger, C., Daëron, M., Huntington, K. W., John, C. M., et al (2019). *Effects of improved ^{17}O correction on interlaboratory agreement in clumped isotope calibrations, estimates of mineral‐specific offsets, and temperature dependence of acid digestion fractionation*. Geochemistry, Geophysics, Geosystems, 20, 3495–3519. https://doi.org/10.1029/2018GC008127.

Poole, F. G., Perry, W. J., Madrid, R. J., & Amaya-Martínez, R. (2005). *Tectonic synthesis of the Ouachita-Marathon-Sonora orogenic margin of southern Laurentia: Stratigraphic and* *structural implications for timing of deformational events and plate-tectonic model. Special Paper 393: The Mojave-Sonora Megashear Hypothesis: Development, Assessment, and Alternatives, 543–596.* doi:10.1130/0-8137-2393-0.543

Reed, B. K. (1959). *Pre-Atokan unconformity of portions of love and Carter Counties, Oklahoma. Petroleum geology of southern Oklahoma*. In J. W. Mayes, J. Westheimer, C. W. Tomlinson, & D. M. Putman (Eds.) (Vol. **2**, pp. 127–141). American Association of Petroleum Geologists.

Rickert, J., Lacroix, B., Moeller, A., Kocsis, L., Vennemann, T., Tatitscheff, B. Absolute timing and related fluid flow associated with the Washita Valley Fault system affecting the Arbuckle mountains, (2024) Geological Society of America Abstracts. doi:10.1130/abs/2024AM-400895.

Ring, U., and Gerdes, A., 2016, Kinematics of the Alpenrhein-Bodensee graben system in the Central Alps: Oligocene/Miocene transtension due to formation of the Western Alps arc: Tectonics, v. 35, p. 1367–1391, https://doi.org /10.1002/2015TC004085.

Roberts, L.R.N, and Kirschbaum, M.A., 1995. Paleogeography of the Late Cretaceous of the western interior of middle North America: coal distribution and sediment accumulation. U.S. Geological Survey Professional Paper, 1561: 1-115.

Roberts, N.M.W., and Walker, R.J., 2016, U-Pb geochronology of calcite-mineralized faults: Absolute timing of rift-related fault events on the northeast Atlantic margin: Geology, v. 44, p. 531–534, https://doi.org/10.1130/G37868.1.

Roberts, N. M. W., Rasbury, E. T., Parrish, R. R., Smith, C. J., Horstwood, M. S. A., & Condon, D. J. (2017). *A calcite reference material for LA-ICP-MS U-Pb geochronology. Geochemistry, Geophysics, Geosystems, 18(7), 2807–2814.* doi:10.1002/2016gc006784

Roberts, N. M. W., Drost, K., Horstwood, M. S. A., Condon, D. J., Chew, D., Drake, H., Milodowski, A. E., McLean, N. M., Smye, A. J., Walker, R. J., Haslam, R., Hodson, K., Imber, J., Beaudoin, N., and Lee, J. K. (2020). *Laser ablation inductively coupled plasma mass spectrometry (LA ICP-MS) U–Pb carbonate geochronology: Strategies, progress, and limitations*. Geochronology, 2(1), 33–61. https://doi.org/10.5194/gchron-2-33-2020

Roberts, N. M. W., Holdsworth, R., Timescales of faulting through calcite geochronology: A review, Journal of Structural Geology, Volume 158, 2022, 104578, ISSN 0191-8141, https://doi.org/10.1016/j.jsg.2022.104578.

Sharp, ZD., (2009) Application of stable isotope geochemistry to lowgrade metamorphic rocks, Blackwell Publishing Ltd., p. 227

Slattery, Joshua & Cobban, William & Mckinney, Kevin & Harries, Peter & Sandness, Ashley. (2013). *Early Cretaceous to Paleocene Paleogeography of the Western Interior Seaway: The Interaction of Eustasy and Tectonism*. 10.13140/RG.2.1.4439.8801.

Spoetl, C., and Vennemann T.W., 2003. Continuous-flow IRMS analysis of carbonate minerals. Rapid Communications in Mass Spectrometry, V. 17, pp. 1004-1006.

Suneson, Neil. 2014. Igneous and tectonic history of the Southern Oklahoma Aulocagen. Oklahoma: Mewbourne College of Earth and Energy.

Tanner, J. H., 1967, *Wrench fault movements along Washita Valley Fault, Arbuckle Mountain area, Oklahoma:* AAPG Bulletin, 51, 126–141, doi: 10.1306/5D25B79B 16C1-11D7-8645000102C1865D.

Taylor, L. T., Minzoni, R. T., Suarez, C. A., Gonzalez, L. A., Martin, L. D., Lambert, W. J., Harrell, T. L. (2021). *Oxygen isotopes from the teeth of Cretaceous marine lizards reveal their migration and consumption of freshwater in the Western Interior Seaway, North America. Palaeogeography, Palaeoclimatology, Palaeoecology, 573, 110406.* doi:10.1016/j.palaeo.2021.110406

Thomas, W. The Appalachian-Ouachita rifted margin of southeastern North America. *GSA Bulletin* 1991;103(3):415431.doi: https://doi.org/10.1130/00167606(1991)103<0415:TAORMO>2.3.CO;2

Trincal, V., Buatier, M., Charpentier, D. *et al.* Fluid–rock interactions related to metamorphic reducing fluid flow in meta-sediments: example of the Pic-de-Port-Vieux thrust (Pyrenees, Spain). *Contrib Mineral Petrol* **172**, 78 (2017). https://doi.org/10.1007/s00410-017-1394-5

Turko, M, 2019, Structural analysis of the Wichita Uplift and structures in the southeast Anadarko Basin, southern Oklahoma; University of Oklahoma Dissertation https://shareok.org/handle/11244/322861

Turko, M., Mitra, S., 2020 *Macroscopic Structural Styles in the Southeastern Anadarko Basin, Southern Oklahoma*, Marine and Petroleum Geology, https://doi.org/10.1016/ j.marpetgeo.2020.104863.

Turko, M. & B. Tapp, 2021, A structural analysis of the Washita Valley Fault in the southeast Anadarko Basin; Interpretation 9 (1): T183-T200 https://doi.org/10.1190/INT-2020-0079.1

VanArsdale, R., Ward, C., and Cox, R. *Post-Pennsylvanian reactivation along the Washita Valley fault, southern Oklahoma*. United States: N. p., 1989. Web. doi:10.2172/6069642.

Veizer, J., & Prokoph, A. (2015). *Temperatures and oxygen isotopic composition of Phanerozoic oceans. Earth-Science Reviews, 146, 92–104.* doi:10.1016/j.earscirev.2015.03.008

Webster, R.E., 1980*, Evolution of Southern Oklahoma Aulacogen*: Oil and Gas Journal, February, p. 150-172.

Yonkee, W. A., & Weil, A. B. (2015). *Tectonic evolution of the Sevier and Laramide belts within the North American Cordillera orogenic system. Earth-Science Reviews, 150, 531–593.* doi:10.1016/j.earscirev.2015.08.001

Zheng, Yong-Fei. 1998. "Oxygen isotope fractionation in carbonate and sulfate minerals." Geochemical Journal 33: 109-126